VALIDATION AND ASSESSMENT OF DMSP ELECTRON TEMPERATURES IN THE TOPSIDE IONOSPHERE

THESIS

Bradford S. Green, Captain, USAF

AFIT/GAP/ENP/01M-03

DEPARTMENT OF THE AIR FORCE
AIR UNIVERSITY

AIR FORCE INSTITUTE OF TECHNOLOGY

Wright-Patterson Air Force Base, Ohio

The views expressed in this thesis are those of the author and do not reflect the official policy or position of the United States Air Force, Department of Defense, or the U.S. Government.

AFIT/GAP/ENP/01M-03

VALIDATION AND ANALYSIS OF DMSP ELECTRON TEMPERATURES IN THE TOPSIDE IONOSPHERE

THESIS

Presented to the Faculty

Department of Engineering Physics

Graduate School of Engineering and Management

Air Force Institute of Technology

Air University

Air Education and Training Command

In Partial Fulfillment of the Requirements for the

Degree of Master of Science in Space and Solar Sciences

Bradford S. Green, B.A.

Captain, USAF

March 2001

AFIT/GAP/ENP/01M-03

VALIDATION AND ANALYSIS OF DMSP ELECTRON TEMPERATURES IN THE TOPSIDE IONOSPHERE

Bradford Stephen Green, B.A.

Captain, USAF

Approved:

Devin J. Della-Rose, Maj, USAF
Chairman, Advisory Committee

27/2/01
Date

Thurmon L. Deloney, Col, USAF
Member, Advisory Committee

28 Feb 01
Date

Jan J. Sojka, PhD, Utah State University
Member, Advisory Committee

26/2/01
Date

Acknowledgements

First, I would like to thank Major Devin Della-Rose, my thesis advisor, for his guidance and timely feedback throughout the duration of the thesis effort. Whether it stepping in to help acquire data, brainstorming over my methodology, or answering my onslaught of questions, Maj Della-Rose tirelessly volunteered his time and expertise in support of my thesis.

I would also like to thank my other committee members, Col Thurmon Deloney and Dr. Jan Sojka for providing valuable advice. Col Deloney was able to contribute his Defense Military Satellite Program (DMSP) expertise, while Dr. Sojka, the chairperson of the GAIM initiative, motivated several methods to assess the DMSP electron temperature data for its legitimacy to be ingested in future space environment forecast models. I would also like to thank those students and faculty who helped develop my Space Environment and computer background while here at AFIT. In particular Capt Herbert Keyser injected valuable assistance with UNIX, FORTRAN, and several other inquiries along the way, while Dr. William F. Bailey patiently offered several hours of his time reinforcing the basic concepts of magnetospheric, ionospheric, and plasma physics.

Finally I would like to express my gratitude to several professionals in the Space Environment community who either provided us with the necessary satellite or radar data, or coordinated with those that did on our behalf. This list includes but is not limited to Fred Rich, Phil Erickson, and Peter Sultan from Millstone Hill Observatory, Marc Hairston and Rod Heelis from UT-Dallas, Jan Sojka from Utah State University, and Mary McCready from Sondrestrom Observatory.

Table of Contents

Page

Page

List of Figures

Figure Page

List of Tables

Abstract

Geomagnetic disturbances in the near earth space environment can adversely affect numerous military and Department of Defense (DoD) systems and operations. To improve the prediction accuracy of such disturbances, the Global Assimilation of Ionospheric Measurements (GAIM) working group is spearheading an effort to incorporate near real-time ionospheric measurements into the next generation of space environment forecast models. Since the model software is designed to automate the data ingest process, the need arises to examine and validate the quality of such measurements before being assimilated into such a model. One such measurement to explore, which is the focus of this research, is the Defense Military Satellite Program (DMSP) measured electron temperature (T_e).

DMSP T_e data were validated against near simultaneous incoherent scatter radar (ISR) T_e measurements from Millstone Hill, MA and Sondrestrom, Greenland for a select 43 conjunctions between Winter 1996 and Summer 2000. DMSP T_e measurements for a given overpass were averaged, while ISR T_e values were either averaged or extrapolated, depending on the ISR mode, to determine T_e comparison values. In some cases, instrument related anomalies produced unreliable measurements.

Of the 37 Millstone and six Sondrestrom conjunctions compared, DMSP T_e values exceeded ISR T_e values by an average of about 25 percent, which is nearly three times the mean ISR uncertainty. Photoelectrons collected by the DMSP Electron Probe contaminated T_e values particularly during solar minimum. A more comprehensive

comparison extending to other sectors of the DMSP orbit is required to determine if a DMSP T_e or ISR T_e bias truly exists.

Based on an assumed linear T_e behavior at mid latitudes, the average DMSP T_e random noise level above Millstone Hill was estimated at about four percent, falling well within the published T_e measurement accuracy of 10 percent. This approach was inappropriate to use at high latitudes due to the high variability of ionospheric phenomena over short distances.

VALIDATION AND ANALYSIS OF DMSP ELECTRON TEMPERATURES IN THE TOPSIDE IONOSPHERE

I. Overview/ Problem Statement

Chapter Overview

Further examination of Defense Military Satellite Program (DMSP) electron temperatures will immensely benefit next generation space weather forecast models. This chapter begins by citing the motivation behind validating and assessing DMSP electron temperature (T_e) behavior and its impact on the Air Force Mission. Next, the need to compare Incoherent Scatter Radar (ISR) electron temperature measurements to DMSP electron temperatures is discussed. The scope and general approach of the research is then outlined.

Introduction

The birth of the space age in the late 1950s extended man's operational frontier to include the near-earth space environment. With numerous assets routinely operating in this environment, the Department of Defense (DoD) relies upon accurate and timely warnings of the implications of approaching geomagnetic storms on its space-based systems and on numerous current operations. After over 40 years of research, scientists have learned that the near-earth space environment's composition, density, and dynamics can vary significantly with respect to altitude, latitude, time of day, season, solar cycle,

and geomagnetic activity. Although some progress has been made, the development of space environment forecast models is still in its infancy when compared to its tropospheric counterpart. Today's space models, limited by a delayed input of sparse, sporadic data, often act as more of a "now"cast, or a given day's ionosphere "climo" cast, than as a bona-fide forecast. Just as with tropospheric weather, the most reliable forecast models are those created from ingesting a high geographical coverage of near real-time measurements or observations. With a myriad of both ground and space-based sensors coming on line, there will soon be sufficient data coverage for assimilation into a physics-based, global ionospheric model. Since the deployment of the Special Sensor for Thermal Ions, Electrons and Scintillations (SSIES) instrument (also referred to as the Topside Ionospheric Plasma Monitor) on board DMSP spacecraft in 1987, the capability has existed to obtain near real-time space environment data in the topside ionosphere (to be discussed in Chapter II) at DMSP altitude (approximately 840 km). The Global Assimilation of Ionospheric Measurements (GAIM) working group hopes to assimilate such real-time data along with physics-based algorithms to develop a reliable physics-based global ionosphere model within the next five years *[Schunk and Sojka, 1999]*. One of the key steps in developing such a model is to characterize and monitor the expected data quality, since if bad data are ingested, the resulting ionospheric specifications and forecasts will be poor. DMSP SSIES measurements are one of the several data types GAIM plans to assimilate; with electron temperatures being one of the SSIES measured parameters. Since the model software program is designed to automate the data ingest process, the need arises to validate and investigate the quality of DMSP electron temperature data for incorporation into the GAIM algorithms.

Impact on Air Force Mission

Variations in the near-earth space environment can adversely affect numerous military systems and operations. Increased geomagnetic activity (i.e. from solar flares) can disrupt high frequency radio communications and over-the-horizon (OTH) radars, alter Global Positioning System (GPS) navigation, and charge spacecraft systems to the point of irreversible damage. Due to the ionosphere's impact on these systems, it is critical that a reliable ionospheric forecast model (i.e. GAIM) be developed. The results of this DMSP electron temperature study will directly benefit the GAIM effort as well as Air Force Research Lab's (AFRL) Space Models Branch. A reliable GAIM forecast model could reestablish the standard for Air Force space system protection and optimization.

Problem and Assumptions

The focus of this research involves investigating and statistically quantifying DMSP electron temperature data for biases and quality so that GAIM can adjust their data ingest algorithms. Both ground-based and space-based sensors can measure such ionospheric parameters as electron and ion densities and temperatures. Incoherent scatter radar (ISR) is the primary reliable ground-based measurement tool for topside ionospheric parameters. There are nine ISR sites worldwide (Map of locations in Chapter II) [*Millstone Hill Website, 2000]*. Despite ISR data's sparse, intermittent coverage, we assume it to be ground truth against which the DMSP data are compared. Incoherent scatter radar T_e measurements are taken from the return signal off of ionospheric electrons. Since electron density decreases with altitude above 300 km, ISR returns at

DMSP altitude (840 - 865 km) are quite weak and thus contain a low signal to noise (SN) ratio. Consequently, a large hurdle to our comparison is either missing ISR data or data with large error at higher altitudes.

Meanwhile, the SSIES electron probe mounted on DMSP spacecraft measures the state of ionospheric plasma at the DMSP's orbiting location. The electron probe records continuous measurements during its 101-minute sun-synchronous orbit around the earth. Measurements are taken at all latitudes, several local times, all seasons, and all phases of the solar cycle, but are limited to DMSP altitude (840 – 865 km). With SSIES data continually passed down once per orbit, it is more extensive and encompassing than ISR data. Consequently, the challenge is to determine just how dependable, in terms of its validity, dynamic range, and noise level, the DMSP electron temperature data really are.

Research Scope and General Approach

A previous draft document by Sultan and Rich *[2000]* compares DMSP ion density (n_i) measurements with near simultaneous ISR n_i measurements from Millstone Hill Observatory in Massachusetts. A recommendation at the end of their paper was to pursue a similar DMSP – ISR electron temperature comparison. Consequently, this research involves validating and examining the behavior and quality of DMSP T_e data collected at nearly the same time as ISR T_e data observed during the Plasmaspheric Observations of Light Ions in the Topside and Exosphere (POLITE) campaign periods 1 – 10 that fell between Winter 1996 and Summer 2000. SSIES instruments mounted on DMSP spacecraft F12 – F15 measure the data covering this time frame. The POLITE

observation campaign is a coordinated effort by ISR sites worldwide to maximize simultaneous coverage topside ionospheric measurements.

Our study concentrates on examining DMSP electron temperature data collected while orbiting over Millstone Hill, a representative magnetic mid latitude ISR site, and Sondrestrom, Greenland, a representative auroral latitude ISR station. Following criteria similar to the Sultan and Rich n_i study, coinciding DMSP – ISR electron temperature data sets over Millstone Hill and Sondrestrom are identified for comparison and validation. DMSP data within a five-degree circle of Millstone Hill and one-degree circle of Sondrestrom were extracted and averaged, while interpolating and extrapolating techniques are employed to determine a representative ISR electron temperature value for comparison. Due to the complexity of T_e behavior over high latitudes compared to mid latitudes, our efforts focus more on assessing the DMSP T_e data above Millstone Hill than over Sondrestrom.

Once validated and assessed versus near concurrent ISR data, DMSP T_e data over Millstone Hill are examined for random noise using a simple linear fit approach. This approach is not practical at auroral latitudes due to the short scale lengths of ionospheric phenomena. Cases studies are then presented which examine DMSP T_e behavior for mid-latitude ionospheric phenomena, potential instrument malfunction or error, and SSIES T_e measurement comparisons between spacecraft with similar flyover times. Once unreliable cases are discarded, DMSP T_e trends are cited with respect to noise level, ISR uncertainty, solar cycle, spacecraft, and solar illumination. After these conclusions are drawn from the results, recommendations are made for future work.

II. Background

Chapter Overview

Accurately forecasting variations in the near-earth space environment will help warn of potential impacts to various Air Force and DoD ground and space based systems. This chapter begins with some background information on the near-earth space environment, leading up to electron temperature behavior and the topside ionosphere. Events or conditions that can alter topside electron temperatures are then discussed. These include electron temperature variations with respect to solar illumination, solar cycle, season, latitude and geomagnetic activity. Region specific ionospheric variations such as sub-auroral ion drifts (SAID), and mid-latitude and light ion troughs are then briefly described. Next, the mission and characteristics of DMSP spacecraft are introduced, with emphasis on how the Topside Ionospheric Plasma Monitor (SSIES) measures electron temperatures. Then background details on incoherent scatter radar (ISR) theory and its electron temperature measurement procedure are depicted. Pros, cons, and possible sources of error associated with both DMSP and ISR electron temperature measurement techniques are then cited. This is followed by an overview of the purpose of the POLITE campaign. The chapter concludes with details of some previous DMSP – ISR topside ionospheric measurement comparisons leading up to this DMSP – ISR electron temperature validation study.

The Ionosphere

The near-earth space environment contains a neutral and ionized atmosphere. The neutral atmosphere is the lowest, occupying a region from the Earth's surface to roughly 60 kilometers (km). Just above the neutral atmosphere, the ionosphere makes up the lowest region of the ionized portion of the earth's atmosphere. The other two ionized regions are the plasmasphere and magnetosphere. The ionosphere arises from the interaction between solar radiation and the Earth's atmosphere and magnetic field *[Tascione, 1994]* and extends from about 60 km to beyond 1000 km above the earth's surface. It consists of ions and free electrons created primarily by photoionization of neutral atmospheric species, mainly molecular nitrogen (N_2), oxygen (O_2), and atomic oxygen (O). Even though less than 1 % of the ionosphere is actually ionized, there are sufficiently numerous free electrons and ions to influence the propagation of radio waves. At a given altitude, the ionosphere reflects radio waves below the plasma frequency while allowing waves with higher frequencies to continue to propagate upward.

Ionospheric Density Structure

Electron and ion density, dominant physical and chemical processes, and plasma composition, vertically distinguish the Earth's ionosphere. Electron density (n_e) variation with respect to altitude creates a basic layered structure at all latitudes *[Schunk and Nagy, 2000]*. Consequently the ionosphere is divided into four main layers – D, E, F_1 and F_2. Figure 1 shows typical mid-latitude daytime and nighttime electron density profiles. Notice that electron density exhibits both diurnal and solar cycle variations. The four distinct electron density regions develop due to the differential solar absorption

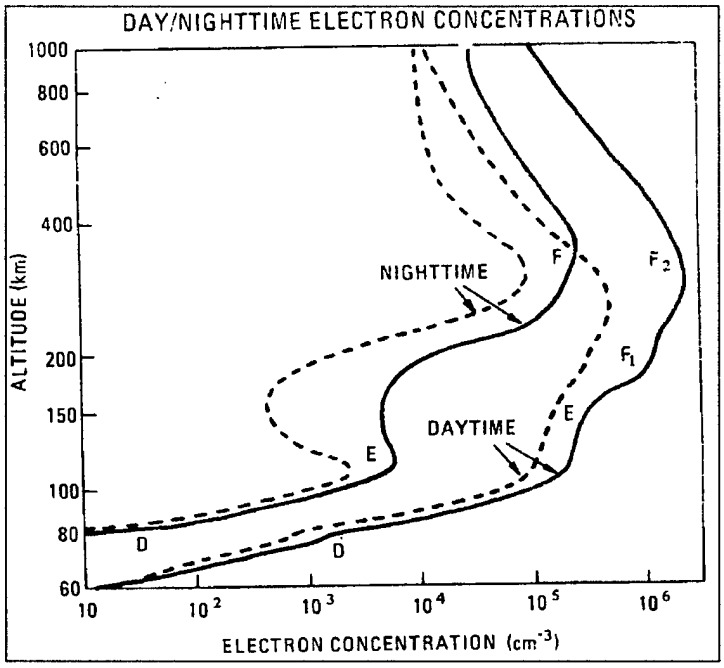

Figure 1. Typical Mid-latitude Daytime and Nighttime Electron Density Profiles. Sunspot maximum and minimum are the solid and dashed lines, respectively *[Tascione, 1994]*.

characteristics of the atmosphere and the resulting different physical and chemical processes unique to each region. In the D and E regions (60 – 150 km), electron density increases with altitude while chemical processes are the most important. Electron densities continue to increase with height in the F_1 region (150 – 250 km) as ion-atom interchange and transport processes start becoming important. The peak ion density of up to 10^6 per cubic centimeter (cm^{-3}) occurs in the F_2 region at around 300 km. Here the ionization maximum occurs due to a balance between plasma transport and chemical loss processes *[Schunk and Nagy, 2000]*. Above this F_2 peak, plasma transport processes and coulomb collisions between plasma particles dominate relative to chemical processes, and electron densities decrease with altitude, eventually becoming monotonic. The topside ionosphere lies in this region above the F_2 peak.

The Topside Ionosphere

The topside ionosphere is the region above the F_2 peak where electron and ion density starts decreasing and where O^+ remains the dominant ion *[Schunk and Nagy, 2000]*. The topside ionosphere ends and protonosphere begins where the lighter atomic ions (H^+ and He^+) begin to outnumber the heavier O^+ ions. The primary reversible ion-atom interchange reaction influencing O^+ versus H^+ densities is:

$$O^+ + H \quad H^+ + O \qquad (1)$$

The O^+ dominant to light ion dominant transition altitude typically ranges from 800 to 1500 km. Consequently, the topside ionosphere extends from around 300 km to anywhere from 800 to 1500 km (See Figure 2).

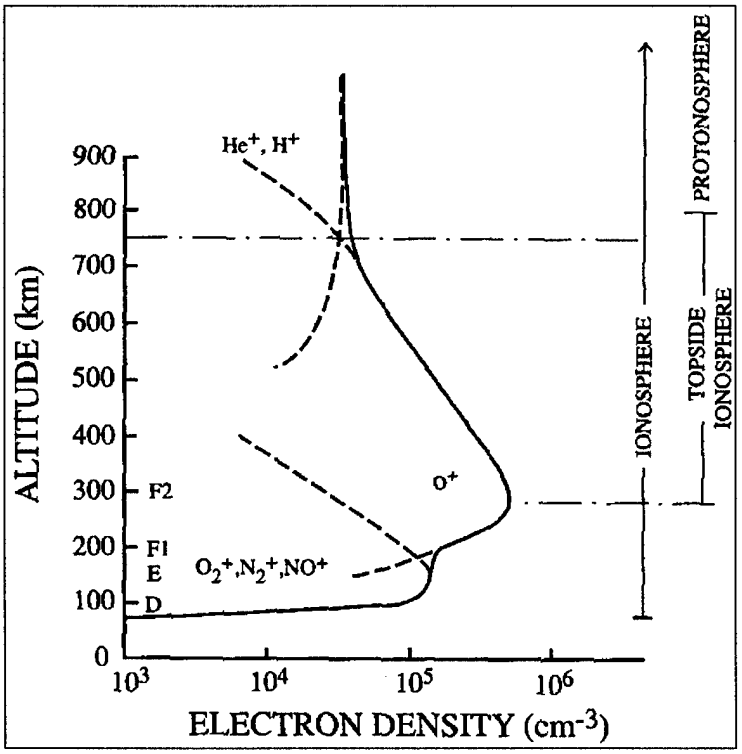

Figure 2. Relative Location of the Topside Ionosphere *[Schunk and Nagy, 2000]*

Historical Context

The existence of the ionosphere was established in 1901 when Guglielmo Marconi successfully transmitted radio signals across the Atlantic Ocean *[Schunk and Nagy, 2000]*. In 1902, Arthur Kennelly and Oliver Heaviside postulated that free electrical charges in the ionosphere could reflect radio waves *[Ratcliffe, 1967]*. The following year, J. E. Taylor suggested that solar ultraviolet (UV) radiation was the source of these electrical charges, implying solar control of radio propagation *[Taylor, 1903]*. The first generally accepted measurement techniques supporting the existence of the ionosphere occurred in 1924 by Appleton and Barnett, and by Breit and Tuve *[Schunk and Nagy, 2000]*. Breit and Tuve's pulse sounding technique could determine the height of a radio pulse's reflection given a signal's frequency. This remote sensing technique generates plots of reflection height versus sounder frequency called ionosondes, which are still widely used today *[Evans, 1975]*. Unfortunately these early ground based ionospheric measurement techniques could only measure ionospheric parameters up to the F_2 region peak at around 300 km. Rocket technology available after World War II, the advent of the Space Age and satellite deployments in the late 1950's, and the emergence of high power pulsed incoherent scatter radar (ISR) around the same time paved the way for observing and measuring physical characteristics in the topside ionosphere.

Electron Temperature

Temperatures of microscopic particles in the ionosphere, namely neutrals, ions, and electrons, are kinetic temperatures, or measures of energy of particles' thermal

motions. Consequently, the average kinetic energy of particles in a gas is directly proportional to its temperature. Temperature is a property of a gas as a whole, not of an individual particle, thus the term "electron temperature" represents a temperature measurement of an electron gas. Thermal energy can be transferred throughout a gas via conduction, convection, or radiation. Thermal conduction, or the transfer of thermal energy by contact, is the dominant means of thermal energy displacement in the topside ionosphere. Photoelectrons from solar extreme ultraviolet (EUV) radiation provide the main source of energy for thermal electrons at all latitudes. These photoelectrons directly transfer energy to topside thermal electrons via coulomb collisions, thus heating the electrons. Higher electron temperatures can generally be expected at high latitudes, where precipitating auroral electrons provide an additional source of energy. Topside thermal electrons lose energy and thus cool via coulomb collisions with ions and downward thermal conduction *[Schunk and Nagy, 2000]*.

Electron Temperature vs. Electron Density Relationship

For a given electron heating rate, the electron temperature is inversely proportional to the electron density. Lower electron densities will lead to greater electron temperatures due to the greater thermal energy available per particle, and less coulomb coupling with ions *[Moffett and Quegan, 1982]*. Conversely, a higher concentration of electrons equates to more electrons sharing a given amount of thermal energy, thus the equivalent electron kinetic temperature is lower. This inverse $T_e - n_e$ relationship does not always hold, as the amount of thermal energy does vary with respect to solar angle (Discussed on page 14), solar cycle, and season. Also the plasma recombination rate,

which reduces n_e, depends non-linearly on T_e, thus a slight increase in T_e can trigger a much larger reduction in n_e *[Sojka, private correspondence, 8 Feb 01]*.

Topside T_e Profile – Diurnal Variation

The main source of ionization and thermal energy for the ionosphere is photoionization *[Schunk and Nagy, 2000]*. Thus when the ionosphere is sunlit and as the solar zenith angle (see page 14) decreases, ionization producing photoelectrons, and photon thermal energy (hν) increase. Typical mid latitude T_e values in the topside ionosphere range from 1200 K (.10 eV) at night to 3500 K (.30 eV) during the day *[Sultan and Rich, Draft Document, 2000]*. This T_e diurnal variation is chiefly due to the photoelectron heat source being shut off at night. At sunrise, T_e and n_e increase rapidly as a result of photoelectron heating and photoionization *[Schunk and Nagy, 2000]*. T_e usually levels off towards midday, and then decreases, as does n_e, towards sunset as the photoelectron heat source disappears. T_e values at topside altitudes normally exceed the temperatures of neutrals (T_n) and ions (T_i). This is primarily based on a conservation of momentum and mass argument, with electrons having the smallest mass, and thus exhibiting the fastest thermal motion and highest temperature of the three species. The higher T_e values can also be attributed to the fact that ion-electron and electron-neutral coupling are low compared to ion-neutral coupling. Figure 3 depicts characteristic day and nighttime T_n, T_i, and T_e profiles up to 800 km over Millstone Hill Observatory while Figure 4 represents an average mid latitude temperature profile up to 4000 km. Notice how T_i comes closer to but never exceeds T_e as altitude increases.

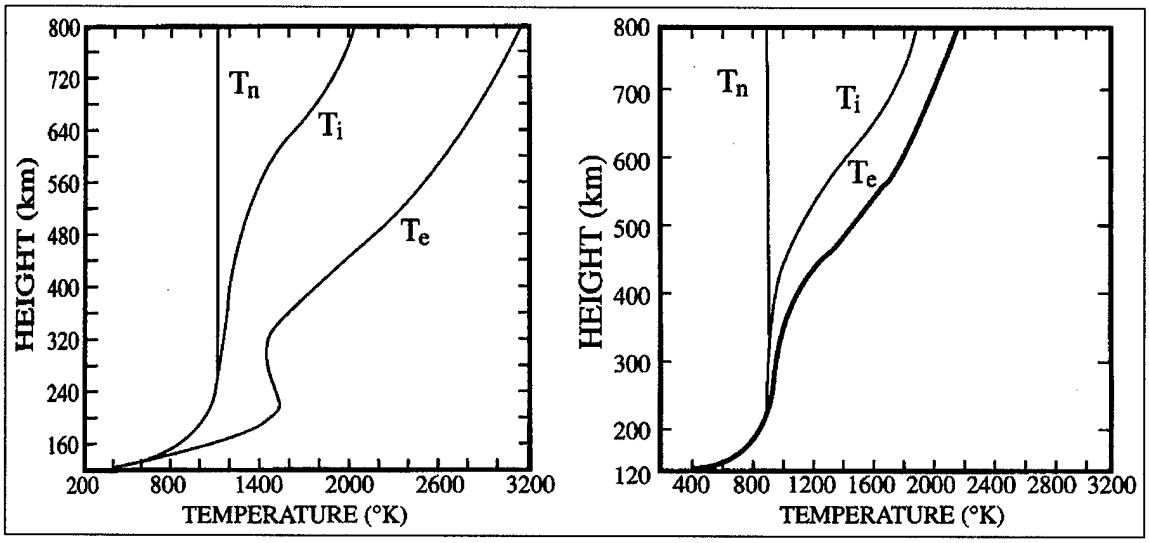

Figure 3. Typical T_e, T_i, and T_n Profiles for Daytime (left) and Nighttime (right) Ionospheres over Millstone Hill on 23-24 March, 1970 *[Schunk and Nagy, 2000]*.

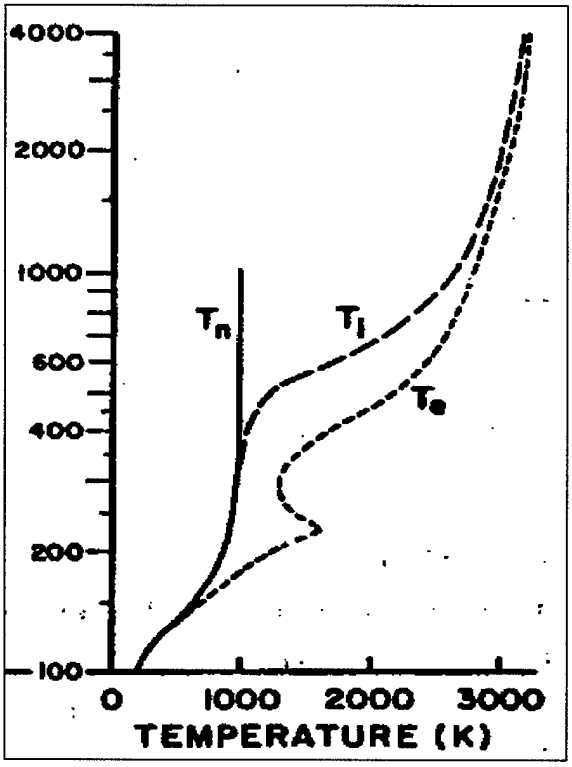

Figure 4. Temperature Profile of a Typical Daytime Mid-latitude Ionosphere. Altitude (km) represents the vertical axis.

Topside T_e Variations

The T_e profile above 400 km, where thermal conduction dominates, usually increases with altitude in response to a downward heat flow from the magnetosphere *[Schunk and Nagy, 2000]*. Topside electron temperatures typically undergo solar zenith angle (SZA) and seasonal variations. The ionosphere's seasonal variation is mainly related to a solar zenith angle change. The SZA is the angle away from which the sun's rays are directly overhead. The solar zenith angle of a satellite orbiting the Earth's ionosphere can be approximated by the angle formed between the sun – center of the Earth line and the center of the earth – satellite line (See Figure 5).

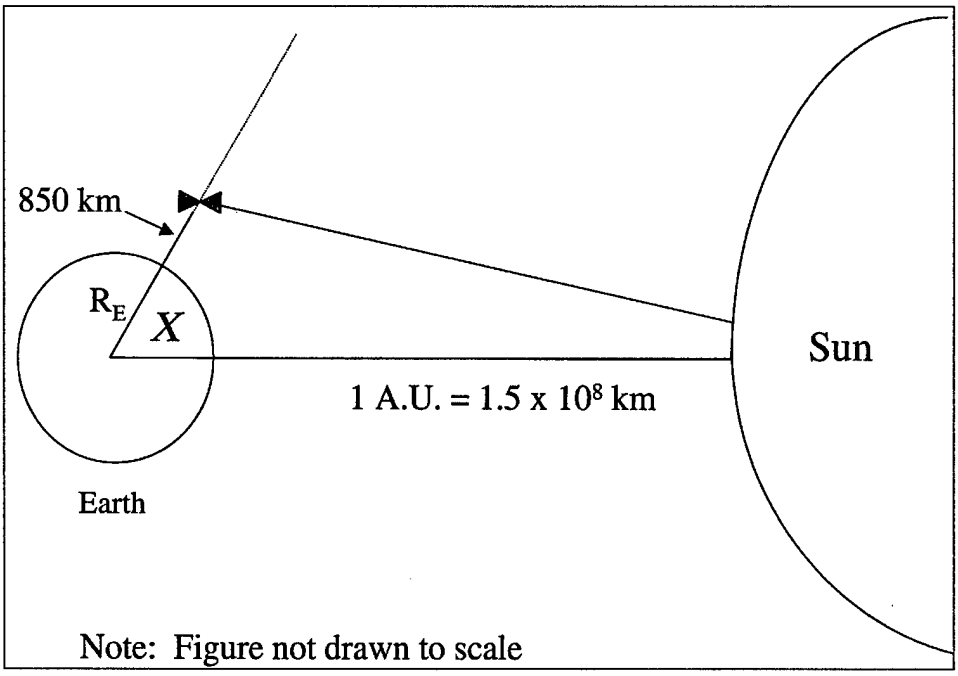

Figure 5. Solar Zenith Angle (X) Determination

Based on an average DMSP orbiting altitude of 850 km, trigonometry was used to calculate the terminator solar zenith angle for DMSP spacecraft to be 118 degrees. A

zero degree zenith angle implies a directly overhead sun, thus a smaller solar zenith angle means more direct sunlight and more frequent photoionization at a given altitude. Thus for a fixed amount of energy, a smaller solar zenith angle results in increased n_e and a corresponding T_e decrease. Conversely a larger zenith angle, as found in the winter hemisphere, suggests less photoionization at a given altitude, lower electron densities and higher electron temperatures for a fixed amount of energy. The overall $T_e - n_e$ correlation is not exclusively tied to solar zenith angle variation. Neutral circulation patterns and thermospheric coupling with the ionosphere create a seasonal anomaly, whose effects can outweigh SZA influence on T_e and n_e *[Schunk and Nagy, 2000]*.

Electron temperatures also vary with respect to solar cycle. The solar cycle is an approximate 11-year variation in the amount of sunspot, solar flare, and geomagnetic storm activity. Solar maximum corresponds to maximum solar activity, while solar minimum signifies the low point of solar activity. At solar maximum, the solar extreme ultra-violet (EUV) radiation fluxes are largest, leading to increased photoionization resulting in higher electron densities and lower electron temperatures. Conversely electron temperatures are higher at solar minimum due to lower electron densities. The solar 10.7 cm radio flux acts as a reasonable estimate for the solar EUV flux *[Rich, DMSP Website, 2000]*. Thus tracking and plotting the 10.7 cm flux trend over several years can reveal the solar cycle pattern (See Figure 14 in Chapter III).

Topside electron temperatures also usually vary with geomagnetic latitude. As mentioned earlier, photoelectrons at topside altitudes transfer energy to thermal electrons by thermal conduction as they stream along magnetic field lines. Photoelectrons have

more of an opportunity to transfer energy to thermal electrons along longer, higher latitude field lines, than along shorter, lower latitude ones *[Schunk and Nagy, 2000]*.

Overall, electron temperatures at high latitudes are characteristically subject to the most variations. At high latitudes, strong electric fields arising from the interaction of the Earth's magnetic field with the interplanetary magnetic field (IMF) produce swift $E \times \frac{B}{B^2}$ ion and electron drifts *[Rishbeth, 1988]*. These drifts increase the likelihood of plasma-neutral collisions that, in turn, induce frictional heating and can elevate ion and electron temperatures. In addition, high latitude geomagnetic field lines can connect to the Earth's magnetotail, allowing for particle precipitation from the tail to enter the topside ionosphere. This incoming auroral precipitation can act as a source of bulk heating and ionization. Electron temperatures increase as a result of these precipitating electrons transferring energy to existing thermal electrons via coulomb collisions that in turn create energetic secondary electrons through ionization *[Schunk and Nagy, 2000]*. On the flip side, the high latitude "open" field lines also allow ions and electrons to escape from the topside ionosphere as well. These aforementioned processes at high latitudes all produce short scale length variations on the topside ionosphere's electron temperature and density structure.

Mid Latitude Ionospheric Phenomena

At geomagnetic mid-latitude regions, where the DMSP – ISR electron temperature comparison above Millstone Hill takes place, T_e behavior is normally quite smooth compared with high latitude T_e variations, but still can deviate due to distinctive ionospheric phenomena. Some uniquely mid-latitude ionospheric phenomena that can

alter mid latitude topside electron temperatures are sub-auroral ion drifts (SAID), mid latitude troughs and light ion troughs.

A SAID event is a latitudinally narrow region (from 0.1 – 2 degrees) of a rapid westward ion drift, located in the evening sector on the equatorward edge of the auroral oval *[Anderson et al, 1993]*. These ion drifts can reach as high as 4 km s^{-1}. A corresponding T_i spike and n_e drop also occur during a SAID. Although SAIDs are most prominent at F_2 altitudes (~ 400km), upward thermal conduction could result in elevated T_e values at DMSP altitude. SAIDs typically occur during the recovery phase of a geomagnetic substorm and last less than three hours *[Anderson et al, 1993]*. During a SAID event, large poleward-directed electric fields develop that can produce westward ion drifts. These enhanced electric fields drive ions to collide with neutrals and then recombine with electrons. This chain of reactions depletes total ion and electron densities while at the same time increasing ion and electron temperatures. The most notable duo of reactions associated with this process is:

$$O^+ + N_2 \rightarrow N + NO^+ \qquad (2)$$

$$NO^+ + e^- \rightarrow N + O \qquad (3)$$

Due to the large thermal conductivity of the topside ionosphere, frictional heating associated with these ion - neutral collisions can contribute to elevated electron temperatures at DMSP altitudes.

Turning to the next mid-latitude feature that can affect electron temperature, according to *Schunk et al. [1976]*, the mid latitude trough (MLT) is a region of low electron density typically found just equatorward of the night side auroral oval. Due to the inverse relationship between T_e and n_e for a given amount of energy, a corresponding

region of elevated T_e may be expected *[Moffett and Quegan, 1982]*. The MLT is most pronounced during fall and winter in the nighttime ionosphere, especially near magnetic midnight. Looking at characteristic MLT morphology, the base of the trough is about four to five degrees of latitude wide, with the poleward trough wall being steeper than the equatorward wall *[Schunk et al., 1976]*. Electron densities in the base on the trough can be on the order of five to ten times lower than those on either side of the trough.

Although the MLT is most evident at lower F-region altitudes, its characteristics are still noticeable at topside altitudes. The processes that can deplete electron densities and thus contribute to the formation of the MLT include the absence of photoionization at night, plasma escape via the polar wind, plasma convection and ion chemistry *[Schunk et al., 1976]*. Both electrons and O^+ are removed from the topside ionosphere by way of the ion chemistry equations (2) and (3) on the previous page, thus supporting MLT n_e trough development *[Schunk et al., 1976]:* The impact that a particular process has on MLT trough formation depends upon a combination of factors such as local time, season, the size of the auroral oval, and the level of past and present magnetospheric disturbances *[Schunk et al., 1976]*.

Another mid-latitude ionospheric feature that can be observed at topside altitudes is the light ion trough (LIT). The LIT is characterized by a pronounced decrease of the light ion (H^+ and He^+) densities, sometimes with little or no corresponding decrease in the electron density (n_e). H^+ and He^+ densities may drop by as much as two orders of magnitude within 5 – 10 degrees of latitude *[Taylor, 1972]*; see Figure 6. Although the LIT can persist during day and night, it is most pronounced during all seasons at night, and during daytime in the winter hemisphere. The steepest gradient heading into the base

of the LIT is typically located near 60 degrees geomagnetic latitude, with a latitudinal extent of 5 – 10 degrees, but can move equatorward and deepen in response to geomagnetic storms *[Taylor, 1972]*. Thus Millstone Hill Observatory, located at 53.2 degrees geomagnetic north latitude, could occasionally be within the equatorward edge of a LIT. Taylor (1972) adds that the base of the LIT appears to mark the average position of the plasmapause, or the boundary separating the more dense plasma (H^+) corotating with the Earth from the less dense plasma affected by magnetospheric electric fields. At the base the LIT, H^+ and He^+ densities can drop by as much as two orders of magnitude to as low as 10^3 ions / cm^3 *[Taylor, 1972]*. No firm conclusion was drawn showing any sort of T_e fluctuation in response to a light ion trough. If the light ions (H^+ or He^+) are the dominant ions at the onset of a LIT, electron temperature can increase in response to LIT development. On the other hand, T_e would show very little variation in response to a LIT if the light ions are the minor ions.

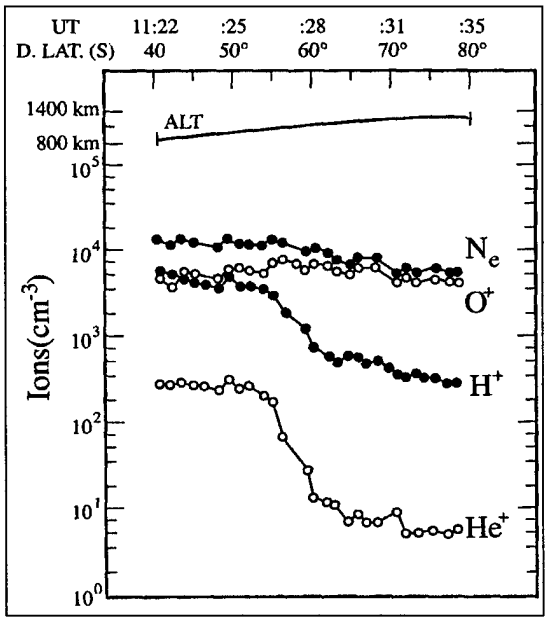

Figure 6. A LIT Measured by the OGO-2 Satellite. Light ion densities can drop an order of magnitude with a few degrees latitude *[Shunk and Nagy, 2000]*.

Incoherent Scatter Radar

Incoherent scatter radar (ISR) is one of the most powerful ground based remote sensing techniques able to provide consistent measurements of the topside ionosphere. An ISR sites transmits shorts bursts, or pulses, of electromagnetic energy to determine the incoherent scatter echo by electrons in the ionospheric plasma. The length of the pulse determines the altitude resolution of the return. The ISR principle is based upon J. J. Thomson's 1906 discovery showing that single free electrons are capable of weakly scattering electromagnetic waves *[Schunk and Nagy, 2000]*. Thus incoherent scatter is often called "Thomson scatter" on his behalf. The term "incoherent scatter" refers to the scattered radar return signal from ionospheric electrons exhibiting random thermal motions. Since the electrons move at varying thermal velocities, the incoherent scatter return echo portrays a Doppler broadened range, or spectrum, of frequencies surrounding the transmitter frequency *[Millstone Hill ISR Tutorial, 2000]*. An extremely powerful radar system is required to detect the weak incoherent scatter echo. This return echo can be as much as 18 orders of magnitude weaker than the outgoing signal (picowatts vs. megawatts).

Determining ISR Electron Temperature

Despite being much weaker than the original signal, the ISR return signal contains valuable information about ion and electron temperature, composition, and velocity. Determining a reliable electron temperature from the weak incoherent scatter signal involves making some key assumptions. First, it is assumed that the ionospheric plasma exhibits a Maxwellian velocity distribution, where particle collisions dominate, and ions

and electrons move at the mean thermal speed ($(\overline{v_i})$ - see Equation 6) *[Schunk and Nagy, 2000]*. Secondly, although incoherent scatter comes from electrons, ions influence electron motions as long as the radar wavelength (λ) is much greater than the Debye wavelength *[Hargreaves, 1992]*. Schunk and Nagy *[2000]* define the Debye length as the minimum distance over which a plasma can exhibit collective behavior. The Debye length is defined as:

$$\lambda_D = \left(\frac{\varepsilon_0 k T_e}{n_e e^2} \right)^{1/2} \tag{4}$$

where

ε_0 = Permittivity of free space

k = Boltzmann constant

T_e = Electron temperature

n_e = Electron density

e = Elementary charge

The incoherent scatter spectrum includes two weak, narrow "electron lines," and a broader, more vivid double peaked ion line power spectrum *[EISCAT Website, 2000]*. Most ISR sites are designed primarily to observe and analyze the ion line spectrum to determine electron temperature. This is based on the assumption that $\lambda >> \lambda_D$, ions influence electron motions, implying that the major portion of the ISR return is concentrated in the ion line *[Schunk and Nagy, 2000]*. Given the Debye length definition above, the Debye length increases as electron densities decrease. As the Debye length approaches or exceeds the radar wavelength, scattering comes from individual electrons, resulting in a Gaussian shaped electron line return instead of the ion line. This could

disrupt the assumed technique of determining T_e from the dual humped ion line return. The twin ion line peaks correspond to Doppler shifts (Δf_i) due to ions approaching the radar at the mean thermal speed ($\overline{v_i}$). Figure 7 below shows such a typical ion line backscatter spectrum where $T_e = T_i$.

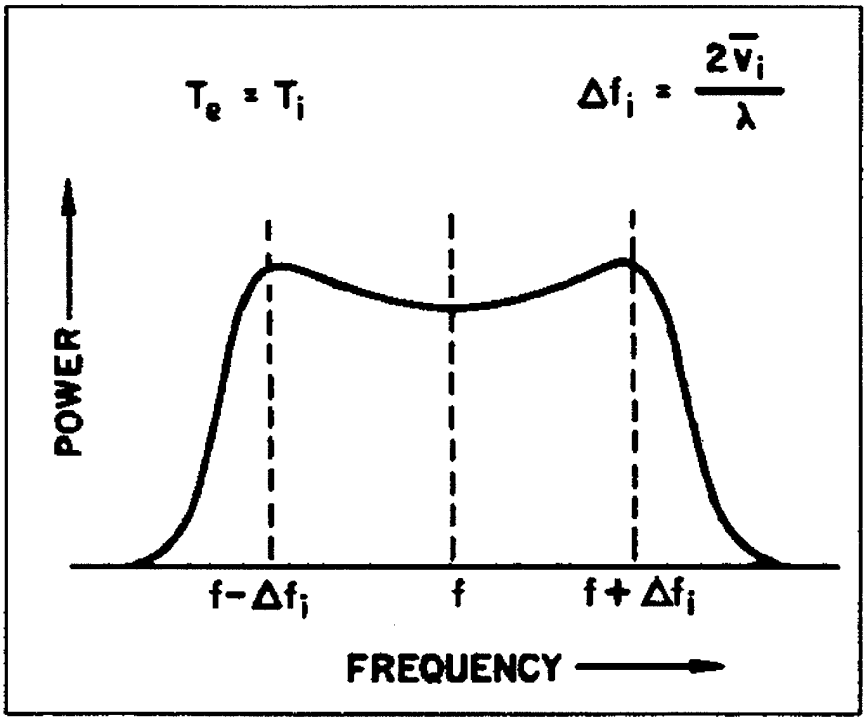

Figure 7. Typical Doppler Broadened Backscattered Ion Line Power ISR Spectrum in the Case Where $T_e = T_i$ *[Evans, 1975]*.

The ion line Doppler shift, Δf_i, dependent upon $\overline{v_i}$, can be expressed as (in Hz):

$$\Delta f_i = \frac{2\overline{v_i}}{\lambda} \qquad (5)$$

where

$$\overline{v_i} = \left(\frac{2kT_i}{m_i} \right)^{\frac{1}{2}} \qquad (6)$$

Substituting for the mean ion thermal speed ($\overline{v_i}$) yields:

$$\Delta f_i = \frac{\left(8kT_i / m_i \right)^{\frac{1}{2}}}{\lambda} \qquad (7)$$

where

k = Boltzmann constant

T_i = Ion temperature

m_i = Ion mass

λ = Radar wavelength

Since ion mass is part of the Doppler shift expression, the ionospheric ion composition is instrumental in determining Δf_i, T_i, and ultimately T_e. Given the above relationships, ion temperature is determined from the width of the twin peaks (as displayed in Figure 7), while the T_e / T_i ratio is extracted from the ion line spectrum shape *[Evans, 1975]*. A wider ion line spectrum indicates higher ion temperatures, and a larger Doppler frequency shift leads to a more shallow ion line spectrum in the center with more pronounced peaks toward the edges *[Millstone Hill ISR Tutorial, 2000]*. Figure 8 shows how the T_e / T_i ratio affects the positive Doppler shift wing of the incoherent scatter echo ion line power spectrum. Once the ion temperature and T_e / T_i ratio are identified, the electron temperature can be easily calculated.

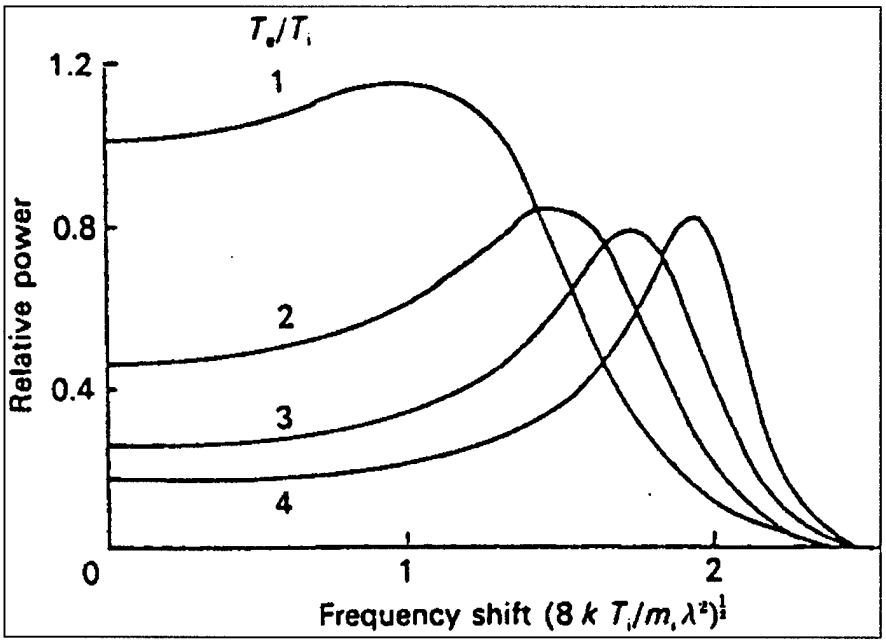

Figure 8. Positive Doppler Shifted ISR Power Spectra for $T_e/T_i = 1$ to 4 *[Hargreaves, 1992]*

Incoherent Scatter Radar Sites

Electron temperature data from two of the nine ISR sites worldwide were used for this research – Millstone and Sondrestrom. Millstone Hill observatory in Massachusetts served as a representative mid-latitude site, while Sondrestrom, Greenland observatory acted as a symbolic high-latitude site. Figure 9 shows a map of all nine locations, and Table 1 reveals coordinate and transmission frequency details for these two ISR sites.

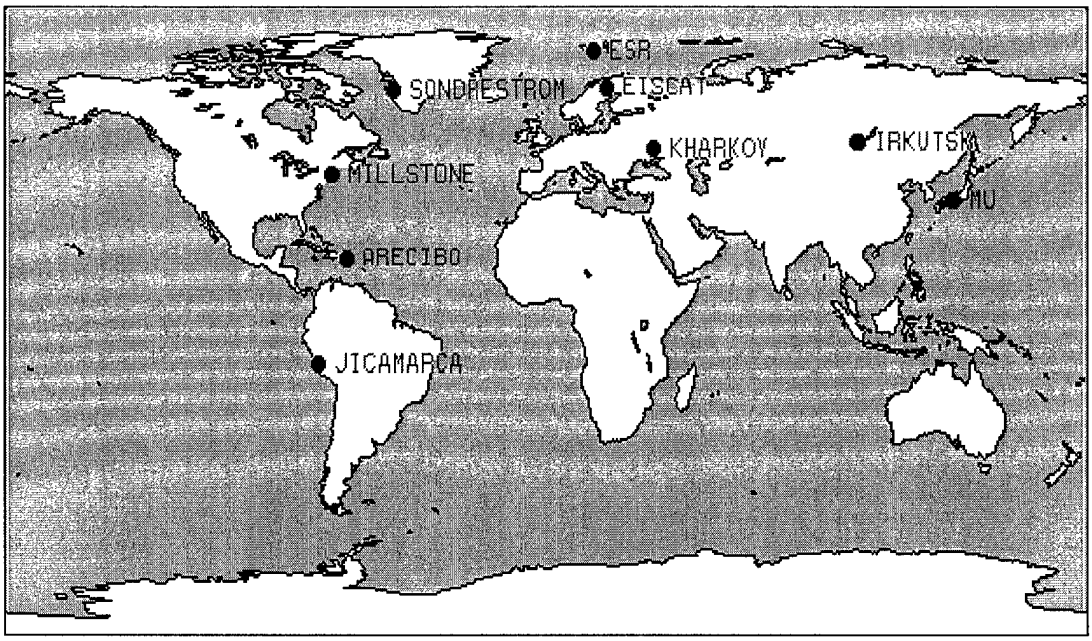

Figure 9. Worldwide ISR Locations *[Millstone Hill Website, 2000]*

Table 1. ISR Sites Used in this Study *[Schunk and Nagy, 2000]*

ISR Site	Geographic Latitude	Geographic Longitude	Geomagnetic Latitude	Elevation Angle	Transmission Frequency (MHz)
Millstone Hill, MA	42.6° N	71.5° W	53.2° N	88°	440
Sondrestrom, Greenland	67.0° N	51.0° W	73.1° N	80°	1290
Sondrestrom "Up B" (@ 850km)	65.9° N	48.8° W	N/A	80°	1290

The Atmospheric Sciences Group (ASG) of the Massachusetts Institute of Technology's Haystack Observatory operates the Millstone Hill ISR observatory *[Milstone Hill Website, 2000]*. ISR measurements began at Millstone Hill in 1960. The ISR instruments there consist of two 2.5 MW 440 MHz transmitters. One is a fully

steerable 46-meter antenna, while the other is a zenith directed 68 meter fixed antenna (see Figure 10).

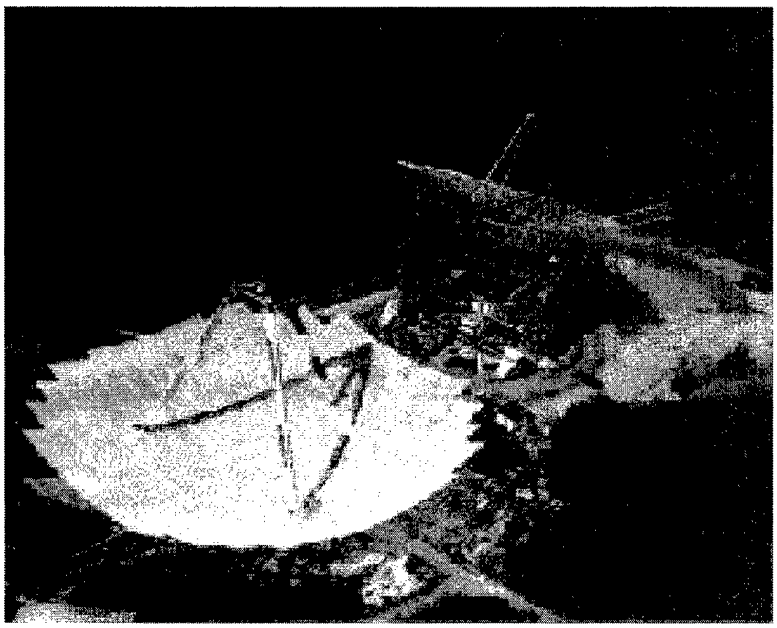

Figure 10. Millstone Hill Fixed Dish (left) and Steerable Dish (right) ISR Antennas *[Millstone Hill website, 2000]*

Millstone Hill's location makes it ideal to study mid-latitude (sub-auroral) ionospheric phenomena and, on occasion, the aurora. Typical Millstone Hill ISR pulse length measurements are at 410, 640, 1000, and 2000 microseconds (μs).

SRI International, based in Menlo Park, CA, operates the Sondrestrom ISR station in cooperation with the Danish Meteorological Institute. The site has been in operation since 1983. ISR data are collected with a 32-meter, fully steerable dish antenna with a 3.5 MW 1290 MHz transmitter (see Figure 11). Sondrestrom's location is ideal for measuring the auroral and sub-auroral ionosphere.

Figure 11. Sondrestrom's 32 m Steerable Dish *[Sondrestrom website, 2000]*

The DMSP Program

Defense Meteorological Satellite Program (DMSP) satellites are a series of sun synchronous polar orbiting satellites that orbit the Earth at altitudes ranging from 840 – 865 km. Each satellite has an orbital period of approximately 101 minutes. A minimum of two spacecraft is usually in orbit simultaneously. The spacecraft are in orbits fixed in local time with equatorial crossing times near 0600 (descending) and 1800 (ascending), and near 0900 (descending) to 2100 (ascending). Table 2 shows equatorial crossing times for the four spacecraft used in this research (F12 – F15).

The primary mission of DMSP spacecraft is to observe tropospheric weather. The secondary mission of DMSP is to monitor the near-Earth space environment. Since 1987, a Topside Ionospheric Plasma Monitor consisting of Special Sensors for Thermal Ions, Electrons, and Scintillation (SSIES) has been mounted on DMSP spacecraft to measure thermal plasma parameters along the satellite flight path.

Table 2. Recent DMSP Equatorial Crossing Local Times (Ascending / Descending) *[Rich, DMSP Website, 2000]*

Satellite	Nominal Local Time of Node	Actual Local Time of Node
F12	2030 / 0830	2049 / 0849
F13	1730 / 0530	1711 / 0511
F14	2030 / 0830	2035 / 0835
F15	2110 / 0910	2110 / 0910

In particular, the SSIES package measures ion and electron density, temperature, sensor potential, ion drift velocity, and He^+, H^+ and O^+ ion composition. Figure 12 below is a schematic of a DMSP spacecraft in its deployed configuration.

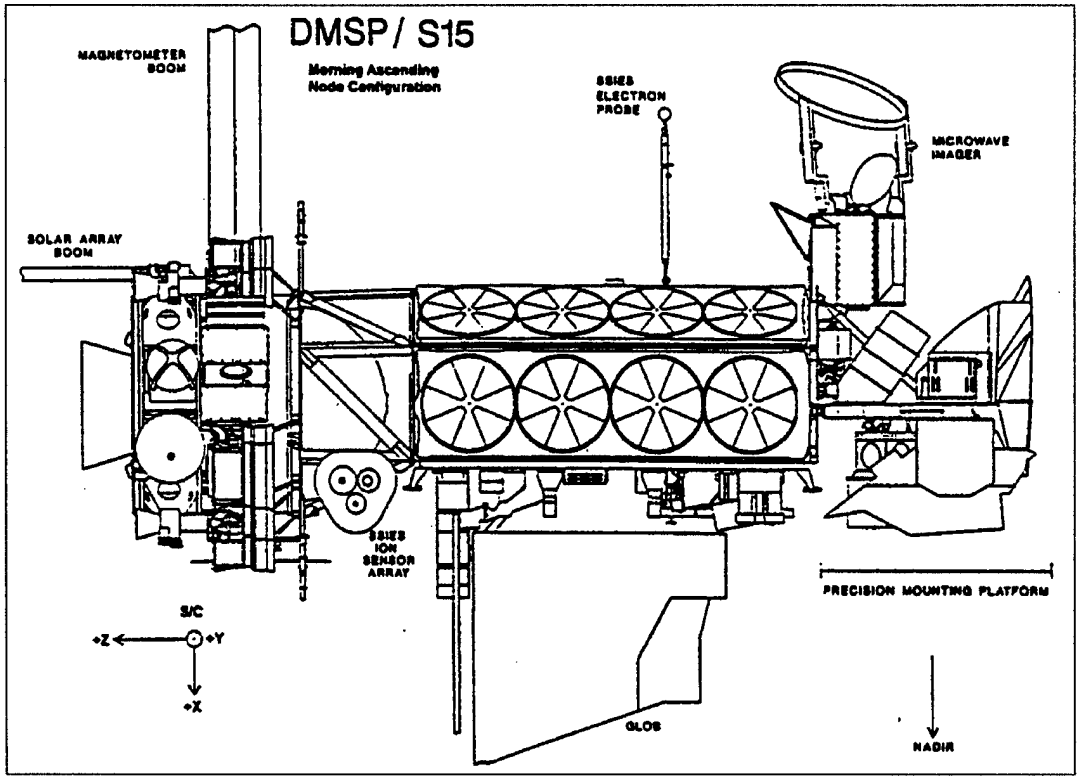

Figure 12. SSIES Sensors Mounted on a DMSP Spacecraft *[Rich, 1994]*

The Langmuir Electron Probe

The specific SSIES instrument that measures electron temperature is the electron probe (EP). This is typically a spherical or cylindrical Langmuir probe engineered to collect charged particles in surrounding environmental plasma. The EP mounted on the DMSP spacecraft is a spherical Langmuir probe designed to measure anticipated electron temperatures at DMSP altitude at all latitudes, seasons, and phases of the solar cycle. With this in mind, the EP measure electrons in the temperature range of 500 – 9000 K to within 10 percent accuracy *[Rich, 1994]*. The EP is mounted on a 2.5-meter boom extending out from the body of the spacecraft to isolate its potential from that of the spacecraft and to minimize collection of unwanted photoelectrons from the body of the spacecraft (see Figure 13). The electron probe weighs 0.2 lbs and consists of an outer gridded sphere of diameter 2.25 inches, and a solid, inner sphere of diameter 1.75 inches.

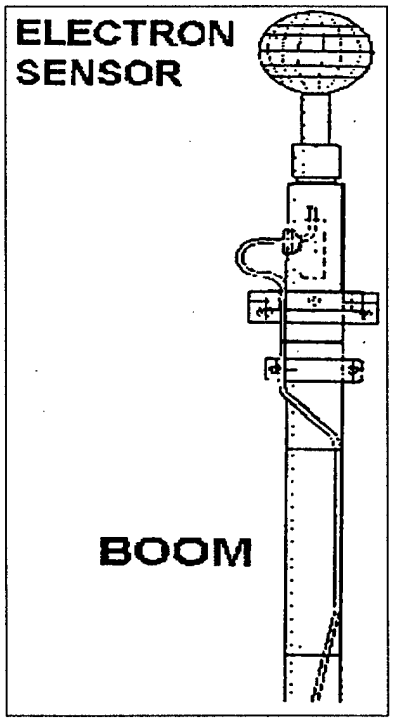

Figure 13. Electron Sensor Mounted on the End of its Boom *[Rich, 1994]*

There is a slight variation of the SSIES electron probe design compared to a standard Langmuir probe. A standard Langmuir probe consists of a standard spherical conducting surface that is directly exposed to the plasma and collects ions and electrons as the probe potential is varied *[Rich, 1994]*. Meanwhile, the SSIES electron probe has an additional outer spherical grid that acts as an electrostatic screen filtering out ambient ions from reaching the charged particle collecting inner sphere. The inner sphere's voltage is electrostatically biased by +20 V to create a positive potential (V_{BIAS}) with respect to the outer grid and spacecraft body to attract electrons through the grid and repel thermal ions. Rich's SSIES Users Guide *[1994]* states that although the outer grid repels the thermal ions, other unwanted charge carriers such as auroral electrons and photoelectrons ejected from the wires of the grid are still collected, possibly contaminating T_e measurements (see "Sources of Error" section, pg. 32). According to Fred Rich's DMSP web site *[2000]*, the EP completes one measurement cycle every 8 seconds, consisting of the potential on the EP grid being swept from –4 V to +4 V and vice versa with respect to V_{BIAS}. Each 4 seconds of data produces one measurement of electron temperature and density. The variation of collected current versus applied voltage helps determine electron temperatures (see next section).

Electron Temperature Determination

Electron temperature is determined from evaluating the logarithmic slope of a best fit line to the electron retarding region of a curve plotting EP collected electron current (I_e) versus EP potential relative to the spacecraft potential *[Schunk and Nagy, 2000]*. Varying the EP voltage and measuring the resulting EP current generates this EP

current versus EP potential curve. The electron retarding region is where the EP potential relative to the spacecraft, or V_p, is less than the plasma potential relative to the spacecraft, V_o. Assuming a Maxwellian distribution of the electron gas, the electron current collected by the EP in the electron retarding region is given by *[Schunk and Nagy, 2000]*:

$$I_e = e\, n_e A \left(\frac{kT_e}{2\pi m_e} \right)^{1/2} \exp\left(-\frac{e|V_p - V_o|}{kT_e} \right) \qquad (8)$$

where

I_e = EP Electron Current

e = Electron Electric Charge

n_e = Electron Density

A = Area of Gridded Sphere

k = Boltzmann Constant

T_e = Electron Temperature

m_e = Electron Mass

V_p = Probe Potential Relative to Spacecraft Potential

V_o = Plasma Potential Relative to Spacecraft Potential

Taking the logarithm of (8) gives:

$$\log I_e = -\frac{e}{kT_e}|V_p - V_o| + \log I_{oe} \qquad (9)$$

where

$$\log Ioe = e n_e A \left(\frac{kT_e}{2\pi m_e} \right)^{1/2}$$

Taking the derivative of (9) with respect to the EP potential gives:

$$\frac{d(\log I_e)}{dV_p} = \frac{e}{kT_e} \tag{10}$$

After eliminating data points caused by photoelectrons and hot electrons, a linear fit is applied to the electron retarding portion of the log I_e vs. V_p curve. The left hand side of (10) represents the slope of this line. Rearranging terms and solving for T_e (in Kelvin) yields:

$$T_e = \frac{e}{k} \times \frac{d(Vp)}{d(\log I_e)} \tag{11}$$

Pros, Cons, and Sources of Error

There are several differences, advantages and disadvantages to each method of measuring parameters in the topside ionosphere. A major difference between the DMSP T_e and ISR T_e measurement techniques is that the DMSP SSIES measures electron temperatures at a relatively constant altitude (840 - 865 km) as time and position vary. Meanwhile the stationary zenith antenna ISR measures electron temperatures at a fixed location above the site as altitude and time vary. Major advantages of DMSP data are its continuous measurement collection capability and better data temporal resolution. With at least two spacecraft in operational at any given time, data can be collected for a minimum of four local times per 101-minute orbit. DMSP processes T_e measurements in

four-second intervals. On the other hand, incoherent scatter radars are only typically turned on for given blocks of time to support funded experiments. ISR data profiles are normally averaged over 2 to 10 minute intervals.

DMSP and ISR each possess possible sources of error unique to each electron temperature measurement technique. Rich's SSIES Users Guide *[1994]* cites the inherent uncertainty of the SSIES electron probe's sensitivity at ± 50 K. Since the DMSP T_e measurement technique depends upon net current collected by the electron probe, unwanted charge carriers that are collected, such as photo and auroral electrons, could contaminate measurements *[Rich, 1994]*. Photoelectrons are generated by any surface exposed to sunlight, while auroral electrons enter Earth's ionosphere especially at times of heightened geomagnetic activity. Rich's SSIES Users Guide *[1994]* also asserts that the contaminating influence of photo and auroral electrons on the total current collected by the EP will be minimal as long as the ambient electron flux exceeds the photoelectron and auroral fluxes. However, at lower ambient electron densities, as during solar minimum, an intense photoelectron or auroral electron flux can elevate the resulting electron temperature measurements. As another possible DMSP T_e source of error, if the spacecraft's sensor potential (SENPOT) cannot be maintained, the SSIES data can become unreliable *[Hairston, private correspondence, 21 Dec 00]*. For SENPOT to function properly, the plasma current to the SENPOT reference surface must exceed the leakage and photoelectron current *[Rich, 1994]*.

Turning to potential ISR T_e sources of error, the number of reliable ISR T_e measurements noticeably fall off around 700 – 800 km due to lower signal strength arising from lower electron densities at and above these altitudes *[Erickson, private*

correspondence, 22 Sep 00]. Consequently, measurements especially at higher altitudes have lower signal-to-noise ratios corresponding to larger associated uncertainties. In addition, some of the underlying assumptions behind the ISR T_e measurement technique may not be met, perhaps leading to inaccurate T_e values. For example, plasma may not demonstrate a Maxwellian velocity distribution in the presence of large electric fields, or at latitudes and altitudes with low electron densities and fewer particle collisions. Also, Millstone ISR data was fit based on a two-ion (O^+ and H^+) composition in the topside ionosphere *[Erickson, private correspondence, 14 Sep 00]*. Any deviation to the assumed O^+ / H^+ ratio could alter the ISR T_e values. Furthermore, recall that at lower electron densities, the Debye length can approach the radar wavelength, generating an ISR return shape exhibiting a more Gaussian than dual-humped shape, possibly leading to incorrect T_e values.

POLITE Campaigns

The Plasmaspheric Observations of Light Ions in the Topside and Exosphere (POLITE) observation campaign is a collaborated effort by ISR sites worldwide to maximize simultaneous coverage of topside ionospheric measurements. Each of the ten POLITE experiments lasted from one to three days between winter 1996 and summer 2000, spanning a time window from solar minimum to solar maximum. Table 3 below shows the exact POLITE experiment dates and times. Although the focus of the POLITE initiative was to observe oxygen, hydrogen, and helium ions in the topside ionosphere, electron temperature and density were measured as well. Since incoherent scatter radars for the POLITE campaigns were set to a mode optimizing returns from the topside

ionosphere, this provided an excellent opportunity to obtain reliable topside electron temperatures.

Table 3. POLITE 1-10 Dates

POLITE	Start Date	Julian Day	Time (Z)	End Date	Julian Day	Time (Z)
1	13-Feb-96	044	1553	14-Feb-96	045	1558
2	11-Nov-96	316	1606	14-Nov-96	319	1639
3	3-Jun-97	154	1204	6-Jun-97	157	1645
4	2-Dec-97	336	1527	4-Dec-97	338	1648
5	26-May-98	146	1605	28-May-98	148	1548
6	22-Nov-98	326	1422	24-Nov-98	329	0137
7	8-Oct-99	281	1550	9-Oct-99	282	1556
8	9-Dec-99	343	1610	10-Dec-99	344	1610
9	6-Jan-00	006	1304	7-Jan-00	007	1637
10	1-Jul-00	183	1255	3-Jul-00	185	1956

Previous Related DMSP Validation Studies

Although numerous studies have been conducted validating ISR topside measurements with *in situ,* or direct, rocket measurements, the concept of comparing DMSP SSIES measurements with ISR parameters is still in its infancy. A past study comparing 24 Millstone Hill ISR topside ion density (n_i) measurements with DMSP F8 and F9 n_i measurements was mentioned in Fred Rich's SSIES User Guide *[Rich, 1994]*. Results of this study revealed that in 80 percent of the cases, DMSP n_i measurements agreed with the ISR n_i measurement to within 20 percent, which was the limit of the ISR accuracy at 840 km altitude. Also, in no case was there a difference greater than 35 percent. Rich and Sultan of Air Force Research Lab's (AFRL) Battlespace Environment

Division later completed a documented, more rigorous Millstone Hill ISR – DMSP n_i study by examining 31 cases of near simultaneous n_i measurements taken between 1989 and 1991 during a solar cycle maximum. The primary result of that study is that SSIES ion densities agree to within a nine percent accuracy of the Millstone Hill ISR ion densities *[Sultan and Rich, Draft Document, 2000]*. A closing recommendation of that research was to pursue a DMSP – ISR T_e comparison study, hence driving this effort. To date, no previous DMSP - ISR T_e comparison and validation studies have been carried out.

III. Methodology

Chapter Overview

This chapter explains how the DMSP and ISR electron temperature (T_e) data are processed, displayed and compared into meaningful, identifiable results. First, a description of the raw DMSP and ISR data is given. The DMSP SSIES provides measurements in four-second intervals without associated error, while Millstone Hill's zenith-directed fixed antenna ISR data arrives in roughly 2 – 10 minute intervals per profile at three different pulse lengths, each with associated error. Meanwhile, Sondrestrom's ISR radar measurements are taken at only one pulse length at 13.5-minute intervals per profile. From these data, DMSP flyover times during the POLITE campaign dates are identified over Millstone Hill and Sondrestrom ISR sites. Then, using a previous DMSP – ISR electron density paper as a guide *[Rich and Sultan, Draft Document, 2000]*, we establish suitable criteria for designating near-simultaneous DMSP – ISR measurements for comparison. Next we employ averaging, interpolating, extrapolating, filtering, and fit techniques to determine the electron temperature values for comparison. Advantages and disadvantages are then depicted for the approach used on each type of data. Subsequently, DMSP data for each conjunction are explored for occurrences of mid-latitude ionospheric features. In addition, cases comparing nearly concurrent DMSP flyover times by different satellites are then examined. Both of these steps are designed to help understand and justify DMSP electron temperature behavior. The chapter concludes with a description of how DMSP random noise over Millstone Hill is assessed and presented.

DMSP Data Description

Dr. Marc Hairston from the University of Texas at Dallas (UTD) supplied the DMSP SSIES data corresponding to the POLITE time windows in chronological files segregated by spacecraft and orbit. As mentioned earlier, the range of all 10 POLITE campaigns extended from Winter 1996 through Summer 2000, thus covering solar minimum through solar maximum. SSIES on DMSP spacecraft F12 – F15 recorded the measurements for this time period (See Figure 14). Note that F-10 and F-11 data were incomplete or not available for this time period.

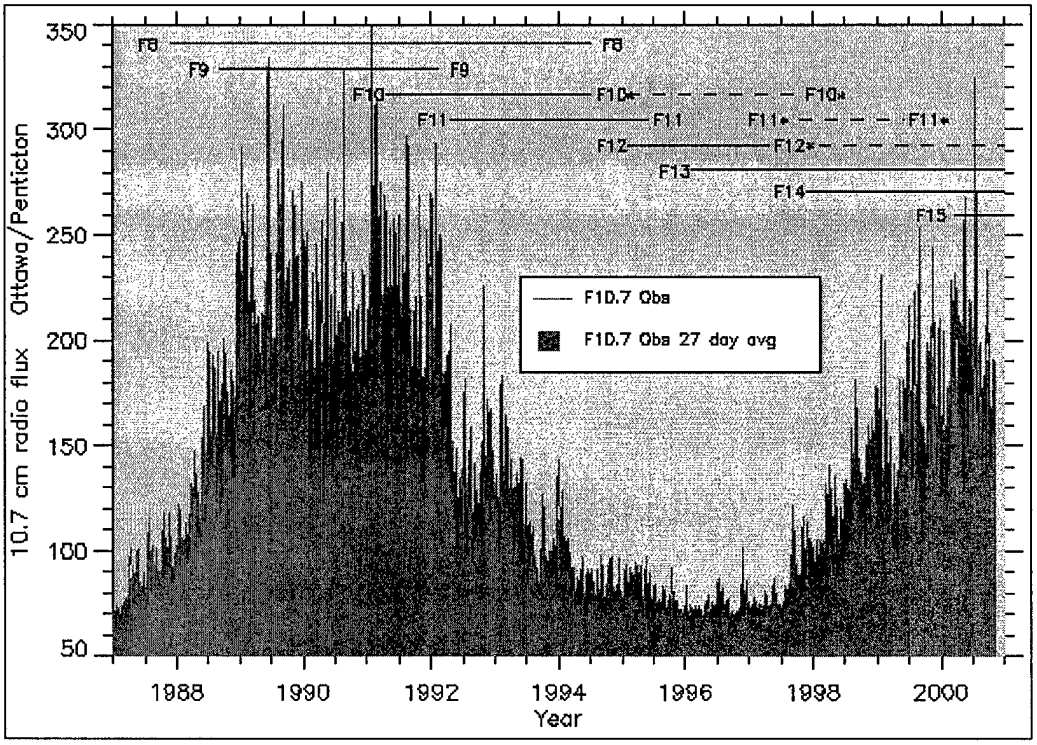

Figure 14. Years DMSP Spacecraft Mounted with SSIES are in Orbit. The corresponding stage of the solar cycle is represented by the F10.7 cm Radio Flux trend *[Rich DMSP Web Site, 2000]*.

Table 4 summarizes the list of SSIES parameters that UTD provided. The data initially contained velocity components (except for POLITE 10), and later included

Table 4. DMSP Data Description

Parameter	Description
Time	Avg. Measurement Time (s)
Vx	X component of Ion Drift Velocity (m/s)
Vy	Y component of Ion Drift Velocity (m/s)
Vz	Z component of Ion Drift Velocity (m/s)
Density	Total Ion Density (cm^{-3})
MLT	Magnetic Local Time
MLAT	Magnetic Latitude
glong	Geographic Longitude
glat	Geographic Latitude
Alt	Spacecraft Altitude (km)
frach	Fraction H^+
frache	Fraction He^+
fraco	Fraction O^+
T_i	Ion Temperature (K)
T_e	Electron Temperature (K)
SZA	Solar Zenith Angle
SENPOT	Sensor Potential (V)

Sensor Potential (SENPOT) and Solar Zenith Angle (SZA) to help determine when the satellite was sunlit. Each complete orbit began and ended as a spacecraft crossed the equator in its ascending node *[Hairston, private communication, 24 Aug 00]*. The data were averaged into four second bins, thus with each DMSP orbit lasting around 101 minutes, each file contained about 1500 data points. Figure 15 shows a representative DMSP T_e plot for an entire orbit.

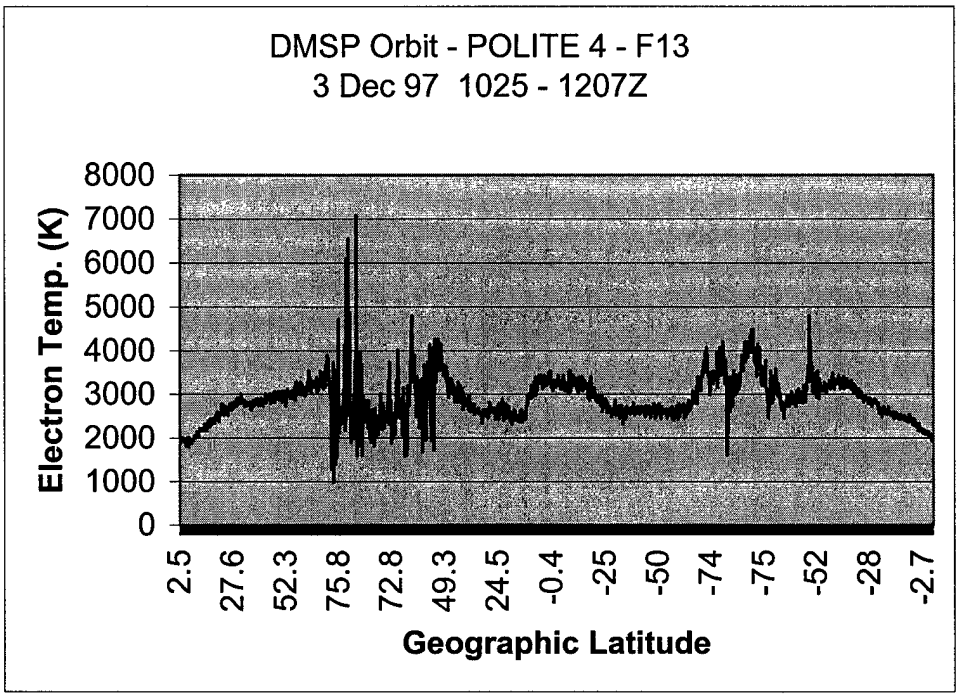

Figure 15. Sample DMSP T_e Data for an Entire Orbit

Before commencing the DMSP T_e analysis, AFRL and UTD advised of potential instrument related factors that could distort some of the T_e data. These included the following:

1. During late 1999 and 2000 (POLITEs 7 – 10), the F14 sensor potential could not remain at the plasma potential during the sunlit portion of the orbit. Consequently, F14 SSIES data is misrepresented for these daylight orbit sectors *[Hairston, private correspondence, 21 Dec 00]*.

2. Due to efforts focused on observing the Leonid meteor shower, all POLITE 6 (22 – 25 Nov 98) T_e measurements were taken in 30-second intervals instead of four seconds. *[Hairston, private correspondence, 21 Dec 00]*. This led to further smoothing of the T_e data.

3. F13 instrument settings could cause evening pass T_e values to be systematically high *[Sultan, private communication, 26 Sep 00]*.

ISR Data Description

Millstone Hill and Sondestrom observatories provided the ISR data for the POLITE 1 – 10 campaigns. Dr. Phil Erickson from Millstone Hill supplied their ISR measurements in 4 different pulse lengths (410, 640, 1000, and 2000 μs) from both the fixed and steerable antennas. To avoid the need to correct for an ISR / DMSP conjunction displacement, only data from the fixed zenith-directed antenna (88° elevation angle) were used for this study. Since most of the 640 μs data was missing, the three remaining ISR pulse lengths were used. Averaged over a smaller altitude extent, the shorter ISR pulse lengths generally have smaller uncertainties and offer finer altitude resolution than the longer pulse lengths *[Erickson, private correspondence, 22 Sep 00]*. The 410 μs pulse length provided the finest altitude resolution (30 km) but only extended up to 751 km, about 100 km shy of DMSP altitude. Meanwhile the longer 1000 and 2000 μs pulse lengths provided measurements well above DMSP altitude, with vertical resolutions of 75 and 150 km, respectively. Table 5 displays details of the three Millstone Hill ISR pulse lengths. Note that each altitude represents the center value of the distance over which the pulse is averaged. For example, a 1000 μs T_e measurement at 874.09 km with a 75 km vertical resolution represents an average T_e value across a 150 km altitude range (± 75 km) centered upon 874.09 km. The ISR data for each pulse length was integrated over a one-minute interval for each profile. Parameters used to analyze Millstone ISR T_e data to compare to SSIES T_e included the following:

1. Time past 0000 UT on the first day of the POLITE campaign
2. Altitude (km)
3. Pulse length

4. Signal-to-Noise ratio
5. Electron temperature
6. Electron temperature error

Table 5. Millstone Hill ISR Pulse Length Details

Pulse Length	**410μs**	**1000μs**	**2000μs**
Low Altitude (km)	152.1	424.7	244.9
High Altitude (km)	751.3	1023.9	1143.8
Vertical Resolution (km)	30	75	150
Points per Profile	21	9	7
Altitude Closest to DMSP (km)	*751.3	874.1	844.1
* Highest Altitude Available			

As the signal-to-noise (SN) ratio decreased with altitude, Dr. Erickson cautioned us to be wary of measurements with SN ratios ≤ 0.1 *[Erickson, private correspondence, 13 Oct 2000]*.

Meanwhile, Mary McCready of SRI provided the Sondrestrom POLITE Campaign ISR measurements at a 450 μs pulse length. Based on McCready's description of the data, each T_e altitude profile was generated from a ten-minute period where the 450 μs pulse sampled the ionosphere every 11.4 km, with the ISR return integrated over a 68 km altitude range parallel to the magnetic (B) field. There was a 3.5-minute time lag between each ten-minute measurement collection cycle. The altitudes covered by these measurements typically ranged from 100 – 1050 km, although most measurements above 500 km were either missing or contained error greater than 15 percent. Parameters used to analyze Sondrestrom ISR T_e data to compare to SSIES T_e included the following:

1. Measurement start time
2. Measurement stop time
3. Altitude (km)
4. Electron temperature
5. Electron temperature error

Extracting Coinciding DMSP – ISR Data Sets

Incoherent scatter radar (ISR) is the only ground-based measurement technique that can provide credible measurements of the topside ionospheric electron temperature. Consequently, DMSP flyovers in the vicinity of ground-based radar sites offer the opportunity to validate DMSP SSIES T_e measurements with near-simultaneous ISR T_e values *[Sultan and Rich, Draft Document, 2000]*.

Overlapping cases were determined by filtering through the DMSP and Millstone Hill T_e data sets to isolate cases where the spacecraft and ISR had measurements similar in time and location given certain cutoff thresholds. Based on Sultan and Rich's *[2000]* recent DMSP – ISR electron density paper, we filtered through the DMSP data set for cases where a DMSP satellite flew within a 5 degree latitude-longitude circle above the Millstone Hill radar site. Using trigonometry, and given Millstone Hill's geographic latitude of 42.62° N, this circle's maximum north to south distance is nearly 1112 km, and its maximum east to west diameter is about 819 km. A FORTRAN program searched for the DMSP measurements lying within such a circle. This routine generated 85 potential DMSP overpasses of Millstone Hill. However, a deficiency of coexisting DMSP and ISR data left only 37 such overpasses feasible for T_e comparison. Since the

spacecraft typically did not fly across the full diameter of the overpass circle, of the 37 total cases, we found anywhere from six to 41 points lying within this circle. Given the four-second interval between data points, this corresponds to the spacecraft being inside this circle anywhere from 24 seconds to 2 minutes 44 seconds per conjunction. Table 6 gives a summary of the 37 cases. Note the case number preceding the dash corresponds to the POLITE campaign, while the second number denotes the chronological occurrence of the conjunction within that campaign. For example, M3-2 denotes the second DMSP flyover within the five-degree circle above Millstone Hill during POLITE Three. The average DMSP flyover time of the points within this five-degree circle was then used to find the corresponding concurrent Millstone Hill ISR data set. Shadowing Rich and Sultan's *[2000]* cutoff criteria established in their DMSP – ISR ion density comparison paper, ISR T_e measurements within ± 30 minutes of the average DMSP flyover time were considered near simultaneous to DMSP measurements within the five degree circle. In addition, at least two sequential altitude profiles within the ± 30-minute time window were required to declare the ISR case as a candidate for comparison with DMSP.

Table 6. Case Summary for DMSP – Millstone ISR T_e Comparisons

Case #	POLITE	YearDay	Time (Z)	Satellite	Points Inside 5° Circle
M1-1	1	96045	0144	F12	41
M1-2	1	96045	1047	F13	29
M2-1	2	96317	1501	F12	31
M2-2	2	96318	1449	F12	41
M2-3	2	96319	1436	F12	36
M3-1	3	97154	1427	F12	18
M3-2	3	97155	0154	F12	13
M3-3	3	97155	1050	F13	29
M3-4	3	97155	2218	F13	22
M3-5	3	97156	0142	F12	39
M4-1	4	97337	1103	F13	40
M4-2	4	97337	1400	F14	39
M4-3	4	97337	1423	F12	26
M4-4	4	97338	1051	F13	26
M4-5	4	97338	1347	F14	38
M5-1	5	98147	0055	F14	39
M5-2	5	98147	1053	F13	27
M5-3	5	98147	2221	F13	23
M5-4	5	98148	1042	F14	34
M6-1	6	98327	0038	F14	11
M6-2	6	98327	1114	F13	40
M6-3	6	98327	1414	F12	37
M7-1	7	99282	0059	F14	41
M7-2	7	99282	0114	F12	27
M7-3	7	99282	1100	F13	24
M8-1	8	99344	0121	F14	15
M8-2	8	99344	1134	F13	24
M8-3	8	99344	1404	F12	22
M9-1	9	00006	2226	F13	28
M10-1	10	00183	1348	F14	29
M10-2	10	00183	1434	F15	39
M10-3	10	00183	2208	F13	40
M10-4	10	00184	0115	F14	22
M10-5	10	00184	1421	F15	12
M10-6	10	00184	2156	F13	21
M10-7	10	00185	0102	F14	40
M10-8	10	00185	0146	F15	32

The same five-degree circle search routine was used to identify DMSP overpasses above the Sondrestrom radar site. This yielded 169 potential cases, of which 56 had corresponding ISR data available. To account for the short scale length and large variations of ionospheric phenomena typical at auroral latitudes, the five-degree circle was reduced to one degree. Since Sondrestrom's ISR signal points up the magnetic (B) field line with an approximate elevation angle of 80°, this one-degree circle was slightly offset from being directly above Sondrestrom's location to account for the departure of the beam from vertical. The smaller circle resulted in 15 DMSP flyovers, seven of which had corresponding ISR data. Table 7 shows a breakdown of these seven DMSP – Sondrestrom conjunctions. Typically three to six data points were found within the circle

Table 7. Case Summary for DMSP – Sondrestrom ISR T_e Comparisons

Case #	POLITE	Spacecraft	YearDay	Time (Z)	Pts. Inside 1° Circle
S2-1	2	F12	96316	2324	6
S3-1	3	F14	97156	2222	6
S3-2	3	F13	97157	1018	5
S5-1	5	F14	98146	1320	5
S6-1	6	F14	98328	2238	6
S8-1	8	F13	99343	1957	3
S9-1	9	F13	00007	1039	4

for a given flyover. The variability of the DMSP T_e data even within this one-degree circle can still be rather large to analyze confidently. Figure 16 shows such an example of a Sondrestrom case.

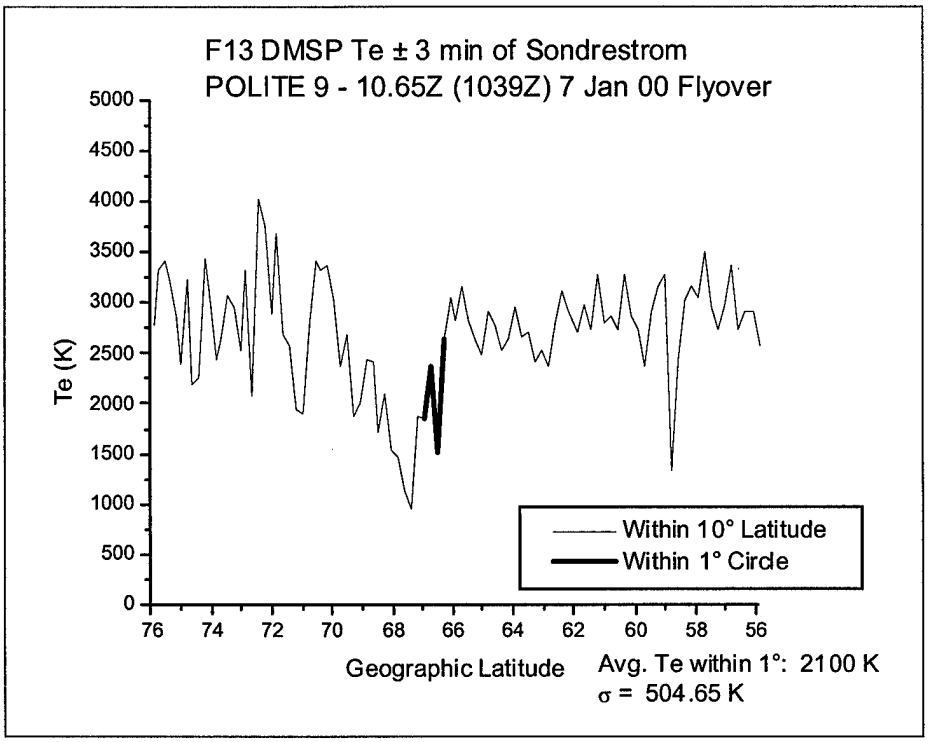

Figure 16. DMSP (F13) T_e Data Near a Sondrestrom Flyover on 7 Jan 00. Notice the large T_e variability over a short distance typical at auroral latitudes (About a 1000 K fluctuation within 1° of Sondrestrom (Bold Line)).

In Figure 16, the standard deviation (σ) of 504.65 K within the one-degree circle of Sondrestrom more than doubles the average σ of 242.93 K calculated for the 37 cases of DMSP T_e measurements within the 5 degree circle of Millstone Hill. Consequently it is much more difficult to distinguish between noise related and physics related T_e behavior at high latitudes than at mid-latitudes.

Calculating DMSP T_e Comparison Values

Once the 37 DMSP – Millstone ISR conjunctions were identified, average T_e values were calculated to determine the final T_e comparison values. The DMSP values used for comparison merely involved averaging the T_e measurements that fell within the five-degree circle for each case. Table 8 below shows mean DMSP electron temperatures

for each case. Note that the T_e values obtained for Cases M8-3, M10-1, M10-4, and M10-7 are unrealistic, most likely due to a probable SENPOT error to be discussed in Chapter IV. Case-by-case plots of DMSP T_e measurements over Millstone Hill are available as a supplementary document upon request.

Table 8. Mean DMSP T_e Value Case Summary

Case #	Satellite	Mean T_e (K)	Case #	Satellite	Mean T_e (K)
M1-1	F12	2921.0	M6-1	F14	2974.5
M1-2	F13	2809.7	M6-2	F13	3455.0
M2-1	F12	4988.4	M6-3	F12	3693.5
M2-2	F12	4522.9	M7-1	F14	2486.8
M2-3	F12	4716.7	M7-2	F12	2580.7
M3-1	F12	4356.7	M7-3	F13	3505.8
M3-2	F12	3211.5	M8-1	F14	3129.3
M3-3	F13	4071.7	M8-2	F13	3005.8
M3-4	F13	3856.4	[1]**M8-3**	F12	**5592.7**
M3-5	F12	3412.8	M9-1	F13	3318.6
M4-1	F13	2960.5	[1]**M10-1**	F14	**811.0**
M4-2	F14	4146.2	M10-2	F15	4144.6
M4-3	F12	4223.8	M10-3	F13	3469.0
M4-4	F13	2903.1	[1]**M10-4**	F14	**779.1**
M4-5	F14	4404.2	M10-5	F15	3895.0
M5-1	F14	2702.6	M10-6	F13	3305.7
M5-2	F13	4084.4	[1]**M10-7**	F14	**772.0**
M5-3	F13	3821.7	M10-8	F15	2839.4
M5-4	F14	2822.4			

Notes: [1] Probable SENPOT error.

Similarly, the mean DMSP electron temperature for the seven possible Sondrestrom cases was calculated by averaging the data points within the one-degree circle ("up B") the same way; Table 9 reveals these values.

Table 9. Sondrestrom Mean DMSP T_e Value Case Summary

Case #	Satellite	Mean T_e (K)
S2-1	F12	2100.0
S3-1	F14	2726.7
S3-2	F13	1780.0
S5-1	F14	3824.0
S6-1	F14	4320.0
S8-1	F13	4036.7
S9-1	F13	2160.0

Calculating Millstone ISR Comparison Values

Determining the average ISR T_e values at DMSP altitude for each case involved a combination of averaging, fitting, interpolation, and extrapolation techniques depending on the ISR mode. On average, about 15 profiles from the 1000 μs and 2000 μs data sets fell within the ± 30 minutes of DMSP flyover time, compared to typically three or four profiles for each 410 μs data set. The maximum altitude and vertical resolution of each pulse length's data helped dictate the method used to compute an average T_e value at DMSP altitude (refer back to Table 5).

Since the 410 μs profiles do not extend up to DMSP orbit altitude (840 – 865 km), extrapolation using a simple curve fitting routine was required to estimate T_e values. Note that associated T_e error was not extrapolated with the T_e measurement due to the complexity of such a procedure. Due to a small signal-to-noise (SN) ratio and corresponding larger uncertainty at higher altitudes, a data "filter" was applied to boost prospects for a more meaningful comparison to DMSP T_e values. A FORTRAN program searched through the 410 μs profiles already within ± 30 minutes of DMSP flyover time for T_e measurements that met the following criteria:

1. SN ratio ≥ 0.1
2. T_e error < 10 percent relative error
3. $T_e + T_e$ Error T_e at the next lowest altitude (i.e., T_e should not decrease with altitude.)

In addition, to carry on with the extrapolation, there had to be at least two resulting "filtered" T_e vs. altitude profiles, each with at least one data point above 450 km. Figures 17 and 18 represent examples of "unfiltered" and "filtered" 410 μs profiles, respectively, for a given conjunction. Filtering eliminated most of the higher altitude points with large error, leaving behind more reliable profiles for extrapolation.

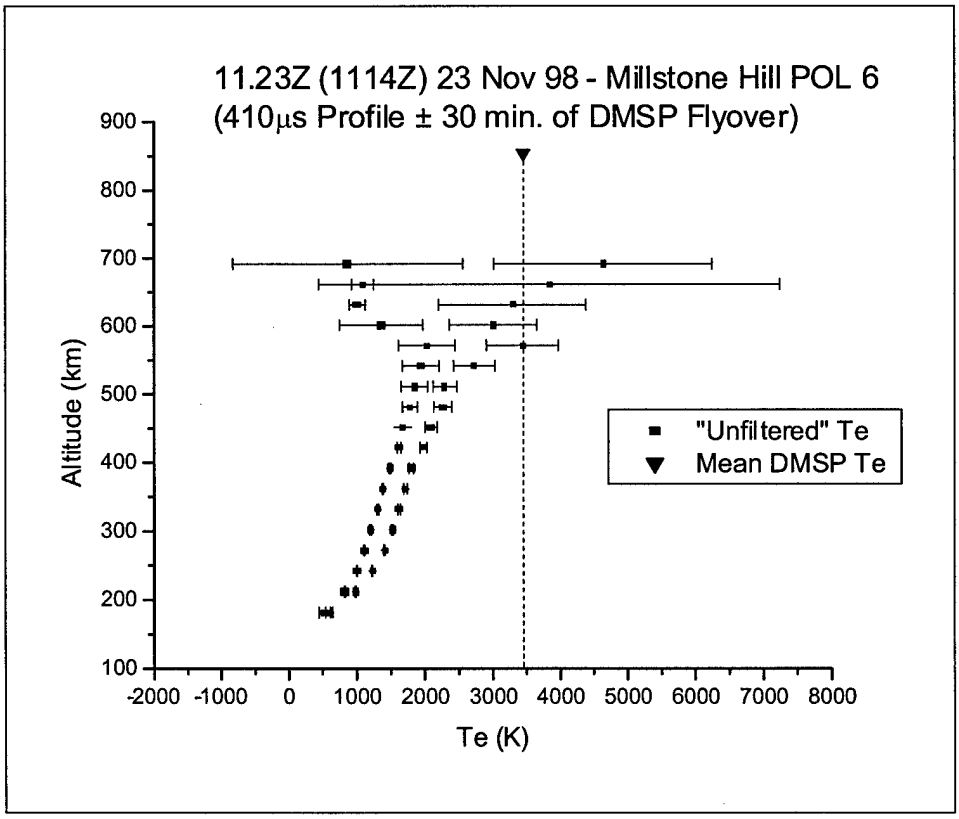

Figure 17. "Unfiltered" 410 μs T_e Data

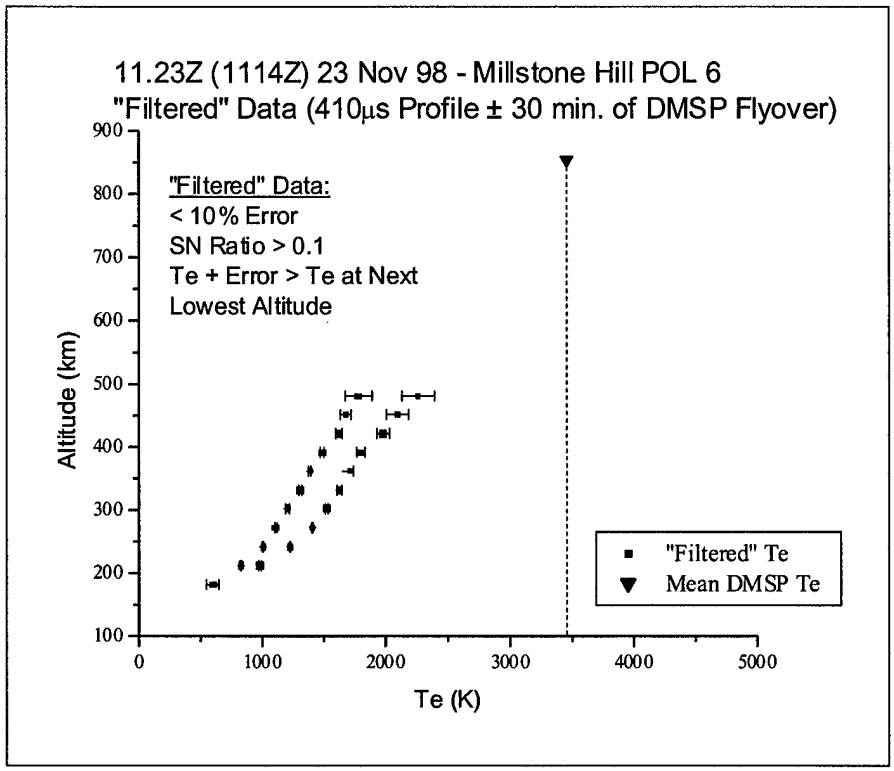

Figure 18. Filtered 410 μs T_e Data

A simple curve fit using Table Curve2D© software provided an extrapolated T_e value to DMSP altitude for each "filtered" T_e profile. For several cases, some of the lower altitude points, especially below 200 km, were removed to provide the most representative fit through the majority of the topside data. If all the T_e profiles for a given conjunction were close enough together upon visual inspection, only one curve fit and extrapolation was performed to determine the T_e comparison value. Otherwise, a curve fit was accomplished on each profile, with the resulting extrapolated values averaged to produce the T_e comparison value. Thirty-five of the 37 conjunctions met all of the criteria to compute extrapolated T_e comparison values from the 410 μs profiles. Figure 19 shows an example of the curve fitting and extrapolation process on one

"filtered" 410 μs profile. Appendix B contains a list of averaged 410 μs extrapolated T_e comparison values, while the plots that generated these values are available upon request.

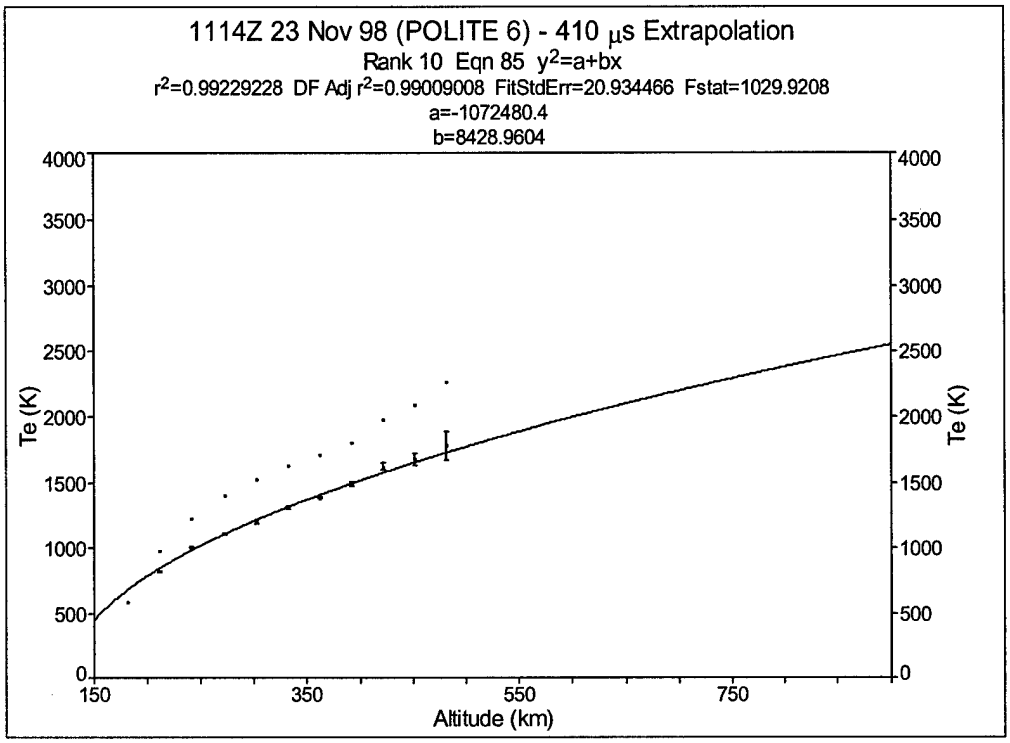

Figure 19. Extrapolation Using a Simple Curve Fit of One of Two "Filtered" 410 μs Profiles Available for a Conjunction. The profile with the error bars is the one being fit. Error is not extrapolated with the T_e measurement. Notice the data point at 182 km is not included to aid in smoothing the fit through the rest of the data points. Extrapolated T_e value at DMSP altitude (854 km) is 2475.11K

Meanwhile, the 1000 and 2000 μs ISR T_e profiles contained the DMSP altitude within its altitude limits, thus averaging pre-existing measurements close to DMSP altitude to generate the T_e value for DMSP comparison was possible. Just as with the 410 μs data, a representative data filter was applied to 1000 and 2000 μs ISR data before any comparison T_e values were calculated. However, this time the T_e data filter was adjusted

to handle the longer pulse length and higher altitude measurements by searching for T_e data meeting the following criteria:

1. T_e error < 15 percent relative error
2. $T_e + T_e$ Error T_e at the next lowest altitude (same as with 410 μs filter)
3. SN ratio threshold ratio not used

These filter thresholds were relaxed slightly compared to the 410 μs T_e cutoff criteria mainly to accommodate reasonable T_e measurements close to DMSP altitude with errors between 10 – 15 percent and/or a SN ratio just below 0.1. Such values would have been dropped under the 410 μs filter thresholds. To support this assertion, Table 10 shows a 1000 μs profile collected during POLITE 6. In this case, the data points at 949 and 1023 km (bolded and shaded) would be removed by both filters, while the data points at 799 and 874 km (bolded) would survive the adjusted filter threshold, but would be removed

Table 10. Filter Application on POLITE 6 Millstone Hill 1000 μs ISR Profile (14.44Z 23 Nov 98)

Time (Z)	Altitude (km)	SN Ratio	T_e (K)	T_e Error	Rel. % Error
14.44	424.67	1.899	2342.2	17.8	0.76%
14.44	499.57	0.767	2603.8	21.3	0.82%
14.44	574.47	0.403	2637.1	44.4	1.68%
14.44	649.38	0.223	2826.0	118.9	4.21%
14.44	724.28	0.135	2916.6	198.3	6.80%
14.44	**799.18**	**0.099**	**3021.6**	**301.6**	**9.98%**
14.44	**874.09**	**0.065**	**3158.2**	**330.0**	**10.45%**
14.44	**949.00**	**0.229**	**2683.0**	**1177.8**	**43.90%**
14.44	**1023.90**	**0.026**	**2874.6**	**91.5**	**3.18%**

by the original 410 μs filter for failing to meet the ≤ 10 percent error and ≥ 0.1 SN ratio requirements. Figure 20 contains a plot for this same profile to show that the 874 and 799 km data points that survive the less restrictive filter appear to be part of the profile trend, thus it seems reasonable to retain such data. Had these points been subject to the tighter filter, averaging and/or interpolating this profile would not have been possible.

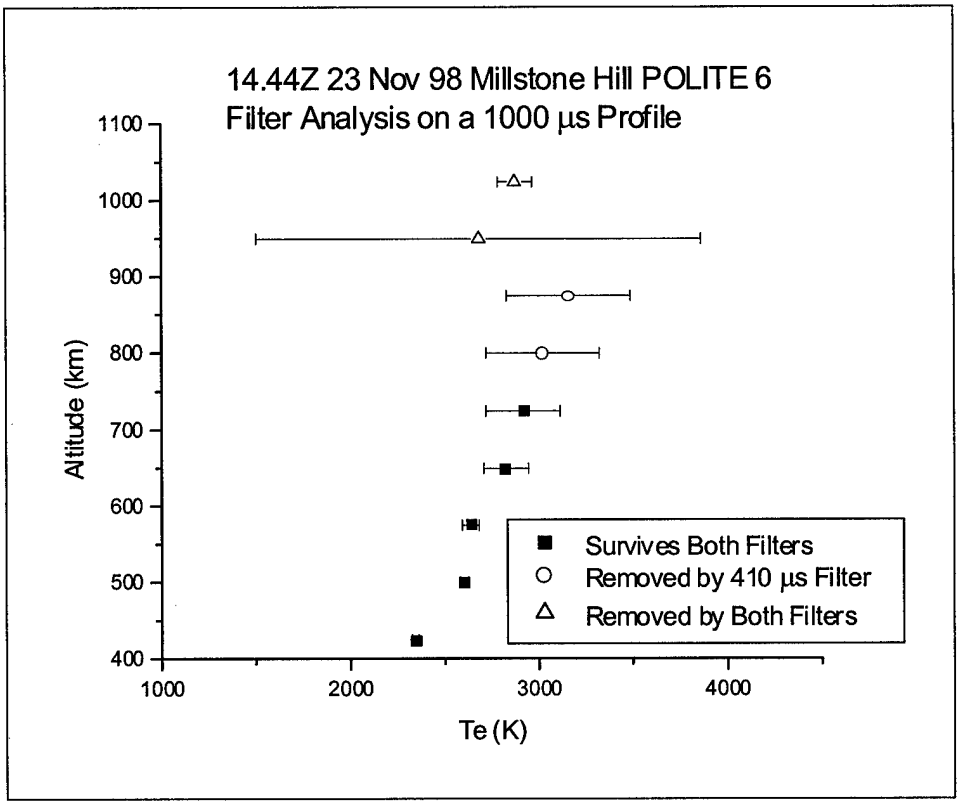

Figure 20. Impact of the Two Filters on a Millstone 1000 μs POLITE 6 Profile. Notice how the more restrictive filter (≤ 10 percent error and ≥ 0.1 SN ratio thresholds) eliminates two points that seem to be part of the profile trend.

On average, ISR electron densities gradually increase to be about one order of magnitude greater during POLITE 10 (solar maximum) than during POLITE 1 (solar minimum) *[Keyser, private correspondence, 12 Feb 01]*. Higher electron densities imply a stronger ISR signal, thus a higher SN ratio and lower absolute error for an ISR

measurement at a given altitude. This n_e versus solar cycle trend perhaps explains why more ISR T_e measurements survive the filtering process towards solar maximum.

The averaging technique for both 1000 and 2000 μs pulse lengths involved extracting and calculating the mean of the "filtered" T_e measurements closest to DMSP altitude. These measurements occurred at 874 km for the 1000 μs data, and at 844 km for the 2000 μs data, while actual DMSP flyover altitudes ranged from 841 – 863 km. Since ISR T_e measurements closest to DMSP altitude are already averaged over a vertical range including the DMSP altitude in the first place, differences associated with averaging at 844 or 874 km versus at the exact DMSP altitude should be small.

To defend this assumption, linear interpolation to DMSP altitude and then averaging the interpolated values was performed on the 1000 μs data to see just how different the T_e comparison results were from averaging at 874.09 km. This procedure was only carried out on the 1000 μs data because the 2000 μs upper altitude bounding DMSP altitude (993 km) required for linear interpolation was usually missing or did not make the filter due to relative T_e error > 15 percent. Linear interpolation was chosen instead of a spline or polynomial fit because the T_e gradient in the 75 km interval containing DMSP altitude is typically quite small *[Erickson, private correspondence, 13 Oct 00]*. For a given 1000 μs profile, linear interpolation to DMSP altitude was only possible as long as the two data points sandwiching the DMSP altitude (874 km and 799 km) survived the filtering process. The average of the resulting linearly interpolated values, as long as there were at least two "filtered" profiles available per conjunction, produced the final Millstone T_e value compared against DMSP. Table 11 shows a comparison of linearly interpolated T_e values to DMSP altitude with T_e values averaged

at 874.09 km. Note that of the 37 total cases, the 16 cases in the table represent those that survived the filtering process, and thus were suitable for interpolation. In all 16 of these cases, the averaged T_e value closest to DMSP altitude exceeded the linearly interpolated T_e average at the exact DMSP flyover altitude (874.09 km) by an average of 52.80 K. This average difference is about five times less than the average absolute T_e error associated with the T_e values themselves. Thus the difference between the two procedures is relatively insignificant.

Table 11. Comparison of Averaging vs. Linear Interpolation Techniques

Case #	1000μs T_e Avg	Avg. Error	[1] 1000μs T_e Lint	Avg. Error	Avg – Lint
M5-1	2139.20	237.86	2133.27	211.09	5.93
M5-3	3028.57	314.05	2994.99	289.61	33.58
M5-4	2266.20	269.96	2230.20	246.20	36.00
M6-3	3131.14	327.80	3027.40	307.45	103.74
M7-1	2475.00	308.03	2420.48	291.46	54.52
M7-2	2456.94	300.83	2366.04	275.49	90.90
M8-3	3014.86	353.60	3011.52	303.95	3.34
M9-1	2766.80	242.70	2756.64	210.90	10.16
M10-1	3576.95	373.36	3464.35	319.57	112.6
M10-2	3637.09	419.75	3511.77	346.78	125.32
M10-3	3209.01	186.32	3151.90	173.19	57.11
M10-4	2376.51	156.68	2330.30	139.76	46.21
M10-5	3166.29	307.09	3154.48	254.37	11.81
M10-6	2868.91	164.75	2830.24	148.11	38.67
M10-7	2437.31	140.64	2383.69	126.11	53.62
M10-8	2170.73	143.50	2109.39	118.49	61.34
Averages	**2795.09**	**265.43**	**2742.29**	**235.16**	**52.80**

Note: [1] "Lint" = Linear Interpolated

Determining Millstone ISR Uncertainty

A representative Millstone Hill ISR uncertainty provides one of the benchmarks against which the overall significance of the DMSP – ISR percent difference can later be compared. Each ISR measurement we received included a T_e value and an associated absolute error, or absolute uncertainty (ΔT_e). Since T_e values are averaged closest to DMSP altitude to determine a mean T_e comparison value for the 1000 and 2000 μs measurements, standard error propagation methods are employed to express a conjunction's T_e comparison uncertainty as the average of individual uncertainties, or explicitly:

$$\left(\Delta T_e\right)_{avg} = \frac{1}{n}\sum_{i}^{n} \Delta T_{ei} \tag{11}$$

where

$\left(\Delta T_e\right)_{avg}$ = Average Absolute T_e Uncertainty

n = Number of ΔT_e Values

ΔT_{ei} = "i^{th}" Absolute T_e Uncertainty Value

Using this method, average ISR T_e uncertainties can be calculated by conjunction, pulse length, and across all pulse lengths. Note that since the 410 μs ISR measurements were extrapolated to DMSP altitude without incorporating error, the overall Millstone Hill ISR uncertainty presented in Chapter IV is only based upon available 1000 and 2000 μs T_e comparison values.

Calculating Sondrestrom ISR Comparison Values

Since most Sondrestrom ISR T_e data from over 500 km were either missing or contained error greater than 15 percent, the smoother lower altitude data profiles were extrapolated to DMSP altitude. Like with the Millstone ISR data, at least two consecutive profiles within ± 30 minutes of DMSP flyover time had to exist for a conjunction to be considered for extrapolation. In addition, a relative error threshold of 15 percent was established as a filtering criterion. Due to the variable structure and limited number of "filtered" measurements available, especially above 500 km, determining an extrapolated average T_e at DMSP altitude proved to be quite complicated.

DMSP – ISR T_e Comparison Statistics

Once DMSP and Millstone Hill ISR T_e comparison values were obtained using the above methods, percent differences between each conjunction's DMSP T_e and each ISR pulse length's T_e value were calculated. In each case, the percent difference was computed according to:

$$\text{Percent Difference} = \frac{(\text{DMSP } T_e - \text{ISR } T_e)}{\text{ISR } T_e} \times 100 \qquad (12)$$

where DMSP T_e and ISR T_e represent DMSP and ISR T_e values, respectively. The average and standard deviation of the percent differences for all cases were then calculated to determine an overall DMSP percent difference and standard deviation compared to the ISR uncertainty and the quoted SSIES T_e measurement uncertainty of ten percent *[Rich, 1994]*. Average DMSP T_e – ISR T_e percent differences are

summarized by pulse length in Chapter IV, and presented by conjunction and pulse length in Appendix A.

Case Study Methodology

Of the 37 Millstone Hill conjunctions, a number of concurrent DMSP T_e and electron density (n_e) profiles were examined to better understand SSIES T_e data consistency, SSIES instrument performance, and to identify ionospheric phenomena that the data revealed. Instances demonstrating SSIES data consistency involved comparing T_e data measured by different spacecraft flying through the same five-degree circle over Millstone Hill within tens of minutes of each other. Occurrences of DMSP T_e profile behavior outside physical and noise level expectations were inspected for possible instrument related anomalies. Meanwhile the structure of simultaneous T_e and n_e profiles were compared to look for such mid-latitude features as light ion troughs, mid-latitude electron density troughs, and subauroral ion drifts (SAID). See Table 18 in the "Results" Chapter for the case summary breakdown.

Determining DMSP T_e Noise Level

As mentioned in the introduction, one of the goals of this research was to assess the DMSP T_e random noise level, as this is crucial information for space weather modeling efforts such as GAIM. The noise level quantification procedure based on a linear T_e variation with latitude represents a first attempt at this objective. DMSP T_e data samples were restricted to the same 37 cases within the five-degree circle above Millstone Hill that were used for the ISR comparison. Consequently, all situations

analyzed were located at mid-latitudes in the vicinity of 42.6 N (53.2 Geomagnetic North). Note that approximating a linear DSMP T_e behavior for the Sondrestrom conjunctions would have been unreasonable due to the short scale lengths of ionospheric behavior at high latitudes. The final statistic obtained to gauge a data set's noise level was the standard deviation as fraction of the filtered mean electron temperature (SDFM). The steps used to obtain the SDFM included the following:

1. Perform a linear regression on the raw data of form: $y = a + bx$.
2. Determine residuals by subtracting the fit from the raw data.
3. Compute the standard deviation of the residuals (σr_0).
4. Remove data points with residuals outside of two standard deviations ($2\sigma r_0$) of the residual distribution. The resulting data set is termed the "filtered" data set.
5. Compute a mean T_e ($\overline{T_{e_1}}$) of the filtered data.
6. Perform a linear regression on the filtered data.
7. Determine residuals from the filtered data.
8. Compute the standard deviation of these residuals (σr_1).
9. Divide σr_1 by $\overline{T_{e_1}}$ to obtain the standard deviation as a fraction of the filtered mean T_e. Thus SDFM = $\left(\sigma r_1 / \overline{T_{e_1}} \right)$.

Based on the assumption that T_e varies linearly with latitude, the simple linear fit was applied with the intent to remove physical trends in the T_e data. Thus any T_e variations around the fit line were considered random noise. Points lying outside the 2σ boundary (Step 4) were assumed to have at least a 95 percent probability of being "bad," and were removed. This procedure is a simplified version of Chauvenet's Criterion for

rejection of data, where a data point is rejected if the probability of its occurrence (based on a Gaussian distribution) multiplied by the number of data points in the set is 50 percent or less *[Mathiesen, 1997]*.

The fact that T_e does not truly behave linearly with respect to latitude poses the risk of poor line fits, which in some cases could filter out T_e data points that appear reasonable. Figures 21 – 24 below graphically step through an example of the DMSP T_e noise level determination process to obtain the SDFM. All SDFM results are presented in Table 18 in Chapter IV.

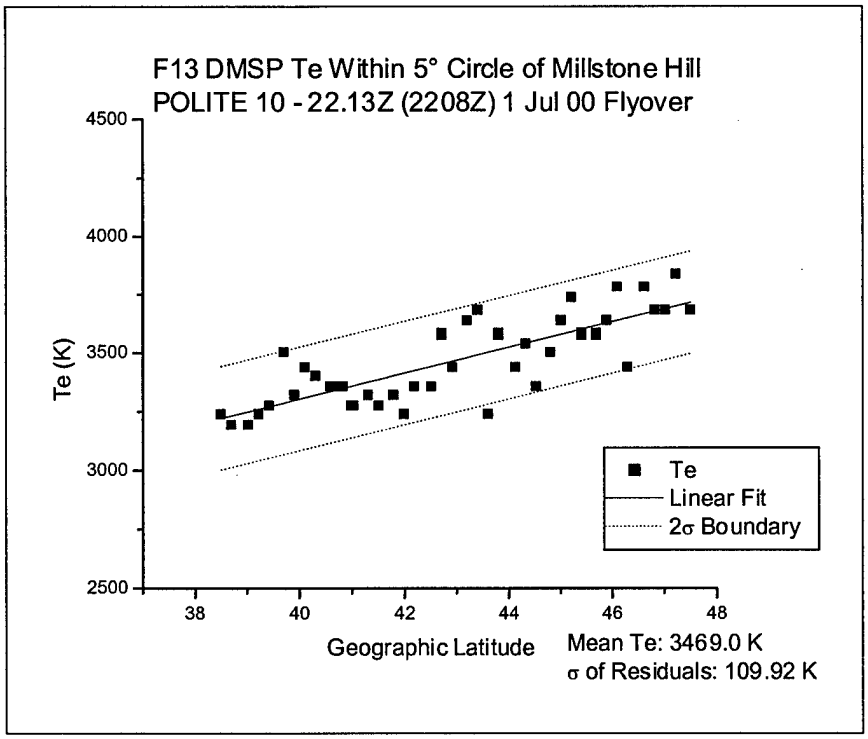

Figure 21. Initial Linear Fit. One point lies outside of 2σ boundary.

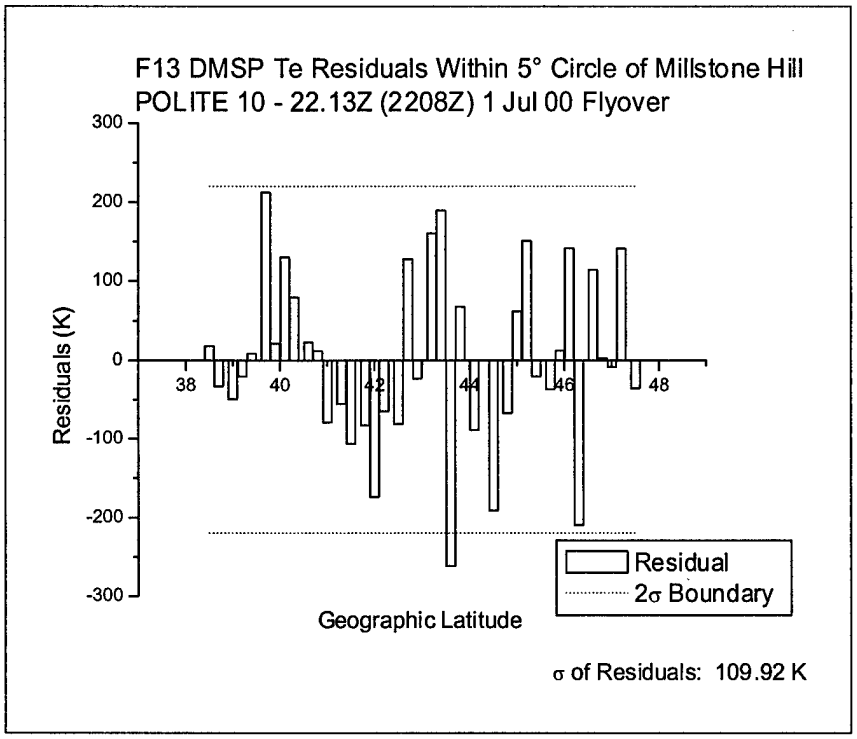

Figure 22. Plot of Residuals Based on Linear Fit. One point lies outside of 2σ, thus is removed before the new linear fit.

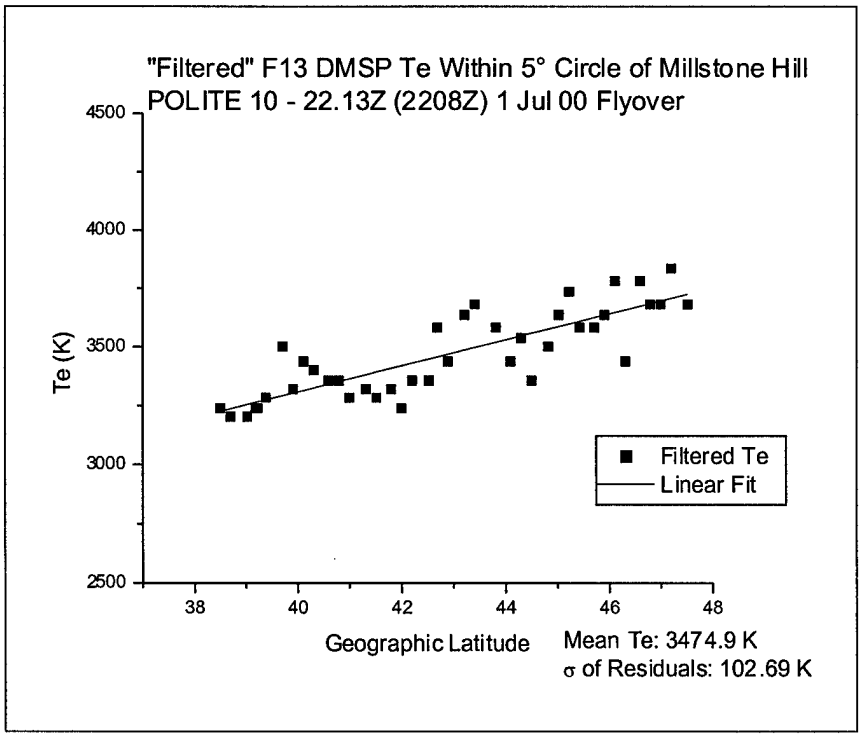

Figure 23. Linear Fit of Filtered Data

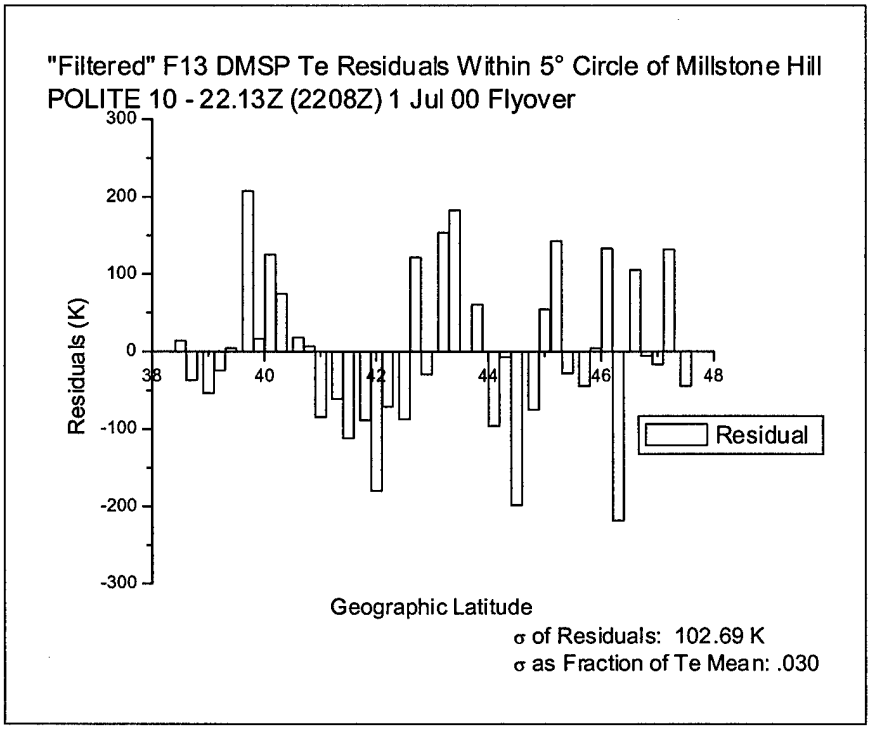

Figure 24. Plot of "Filtered" Residuals

IV. Results and Analysis

Chapter Overview

Averaged DMSP T_e values for all 37 Millstone flyovers and six Sondrestrom flyovers were compared to corresponding ISR filtered T_e estimates at DMSP altitudes. Three DMSP F14 Millstone flyovers during POLITE 10 and an F12 during POLITE 8 produced unrealistic values due to a SSIES SENPOT malfunction and were not included in the result tally. Also, due to missing data, or not enough data surviving the filtering process described in the previous chapter, ISR T_e estimates from all pulse lengths were not obtainable for every conjunction, but there was at least one ISR T_e estimate available per each conjunction. When more than one Millstone Hill ISR pulse length T_e estimate was available, their values lay well within each other's relative error.

The behavior of some DMSP T_e profiles showed indications of possible instrument and telemetry related anomalies that led to extended segments of unrealistic or flat-lined electron temperature values. Nonetheless, the 37 cases of near concurrent Millstone Hill ISR and DMSP electron temperature measurements for the POLITE 1-10 campaigns reveal that DMSP T_e values consistently exceed the complementing raw, filtered, and averaged ISR measurements. The average percent difference between DMSP and Millstone ISR T_e values was nearly 25 percent, exceeding ISR uncertainty by nearly three-to-one. Corresponding DMSP random uncertainties found later in this study (about four percent) do not substantially alter this conclusion. The margin between DMSP and ISR T_e measurements decreases with time from solar minimum towards solar maximum, partially due to a decreased photoelectron influence on DMSP T_e

measurements towards solar maximum. Although high latitude physical variations over short scale lengths can complicate the analysis, a brief look at the seven DMSP – Sondrestrom ISR T_e comparisons show similar results. The nine Millstone instances where an ISR T_e average exceeded its DMSP counterpart happen to occur when there is an argument for faulty SIESS performance or a large uncertainty in the ISR averaging process. Plots and tables supporting these results are found in this chapter and in the appendices. Meanwhile corresponding DMSP electron density measurements are repeatedly lower than the ISR average, verifying the expected inverse relationship between electron temperature and density for a fixed amount of energy *[Keyser, Thesis Draft, 2001]*.

Next, the variability of DMSP measured T_e data over Millstone Hill is assessed to provide a first guess of a mid-latitude random noise level to be considered by GAIM's Kalman filter. In general, the average DMSP electron temperature random noise level for the Millstone Hill conjunctions is under four percent, which is well within the electron probe's published accuracy of 10 percent *[Rich, 1994]*. Details of each case's random noise calculation are presented in a table. Noise level is not determined for the Sondrestrom conjunctions in order to avoid complications caused by the short scale lengths of high latitude ionospheric events.

As part of the DMSP T_e validation process, case studies are analyzed to support specific electron temperature behavior and structure. When comparing T_e profiles from different spacecraft with similar Millstone Hill flyover times, electron temperature measurements are consistent within the aforementioned random noise level. Finally, the chapter closes with a look at some cases showing indications of mid-latitude ionospheric

features such as sub-auroral ion drifts, light ion troughs, and mid latitude electron density (n_e) troughs.

Millstone Conjunctions

Based on the filtering, averaging, and extrapolation techniques introduced in the previous chapter, at least one Millstone Hill ISR T_e estimate could be calculated per conjunction. Of the 37 Millstone Hill conjunctions, thirty-five 410 μs, twenty 1000 μs, and twenty-six 2000 μs filtered ISR T_e values could be calculated. Table 12 shows a case breakdown of these values and associated error. Recall that the 1000 and 2000 μs pulse lengths are averaged to 874 and 844 km, respectively and that 410 μs T_e values do not include an average error due to the complexity of computing an extrapolated average error. The average Millstone Hill ISR uncertainty based on all available averaged 1000 and 2000 μs values was 8.42 percent. Only filtered data were used to determine this ISR uncertainty in order to generate the most representative ISR T_e variation at DMSP altitude.

Due in part to a higher n_e toward solar maximum, more ISR T_e data survived the filtering process from the more recent POLITE campaigns than from the earlier ones. Also, when more than one Millstone Hill ISR pulse length T_e estimate was available for a given conjunction, most of these values lay well within each other's average relative error. This demonstrates a consistency amongst the three pulse length T_e estimates that were compared against DMSP T_e values. The values that did not fall within each pulse length's relative error were typically either based on only two profiles or had SN ratios less than 0.1.

Table 12. Millstone Hill ISR T_e Estimates at DMSP Altitude

Case #	Sat.	DMSP Alt. (km)	410 μs T_e	1000 μs T_e	Avg Error	2000 μs T_e	Avg Error
M1-1	F12	861.87	2207.91	No Data		[2] 3602.15	154.15
M1-2	F13	855.62	*	No Data		[1] 3110.90	222.40
M2-1	F12	846.84	2957.98	*		*	
M2-2	F12	847.57	2600.31	*		*	
M2-3	F12	846.77	2890.01	*		3473.57	450.17
M3-1	F12	860.82	3088.92	*		2905.23	308.40
M3-2	F12	862.35	2905.32	[1] 3074.40	239.75	*	
M3-3	F13	850.13	2530.55	*		*	
M3-4	F13	855.62	*	*		2658.01	279.74
M3-5	F12	863.01	2225.94	[1] 2672.40	243.05	*	
M4-1	F13	860.39	2037.91	[1,2] 3101.05	277.05	*	
M4-2	F14	860.56	3252.33	*		3040.17	424.67
M4-3	F12	847.90	2919.14	*		3298.97	454.17
M4-4	F13	859.50	2457.66	*		*	
M4-5	F14	859.94	3065.20	*		*	
M5-1	F14	857.48	1985.81	2139.20	237.86	1748.98	137.29
M5-2	F13	853.51	3095.07	*		3198.03	357.07
M5-3	F13	859.33	2773.87	3028.57	314.05	2768.52	139.91
M5-4	F14	857.49	2219.99	2266.20	269.96	2125.41	127.56
M6-1	F14	850.07	2888.39	*		*	
M6-2	F13	854.04	2551.80	*		*	
M6-3	F12	846.97	3158.72	3131.14	327.80	3156.74	248.85
M7-1	F14	859.22	2428.68	2475.00	308.03	2364.49	153.89
M7-2	F12	849.39	2349.75	2456.94	300.83	2357.10	160.23
M7-3	F13	854.98	3264.78	*		3269.50	334.13
M8-1	F14	848.18	2548.46	[1] 3802.60	431.60	3380.70	409.87
M8-2	F13	853.77	2742.37	*		*	
M8-3	F12	845.71	3205.74	3014.86	353.60	3184.45	256.80
M9-1	F13	852.12	2511.42	2766.80	242.70	2657.60	111.20
M10-1	F14	846.25	3283.46	3576.95	373.36	3291.50	198.08
M10-2	F15	841.57	3446.84	3637.09	419.75	3412.61	189.27
M10-3	F13	857.97	3010.32	3209.01	186.32	3066.39	97.81
M10-4	F14	853.77	2305.00	2376.51	156.68	2218.76	70.71
M10-5	F15	842.59	3105.89	3166.29	307.09	3066.52	138.30
M10-6	F13	857.48	2801.96	2868.91	164.75	2704.28	89.00
M10-7	F14	853.74	2325.14	2437.31	140.64	2312.87	74.31
M10-8	F15	846.36	2161.87	2170.73	143.50	2013.95	66.07
Cases			**35**	**20**		**26**	
		Avg. T_e (K)	2722.99	2868.60	± 271.92	2861.05	± 217.46
		Relative Error			9.48%		7.60%
		Avg. ISR Uncertainty					**8.42%**

Notes: * N/A

[1] Based upon only two profiles

[2] SN ratio << 0.1

DMSP vs. ISR T_e Comparison over Millstone Hill

Of the 37 Millstone conjunctions, DMSP T_e measurements consistently exceeded the "filtered" ISR T_e estimates for all three pulse lengths. The difference between DMSP T_e and corresponding ISR T_e decreased towards solar maximum. Ten values deviated from this trend (four DMSP and six ISR), probably due to SSIES SENPOT problems and highly uncertain ISR estimates based on only two profiles or with high SN ratios. Figure 25 below shows all available DMSP and ISR T_e measurements for the 37 conjunctions. The DMSP spacecraft involved in each case is shown as the last term of the case number.

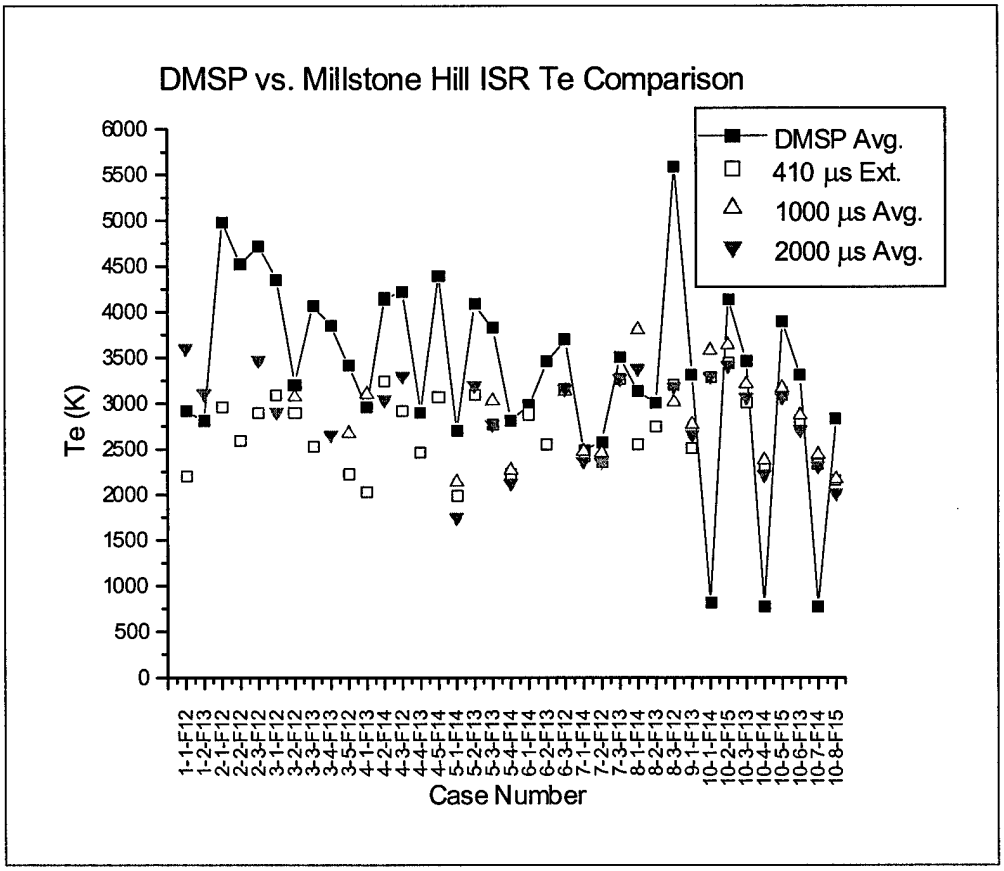

Figure 25. DMSP T_e vs. All Available Millstone Hill ISR Comparison Values. Note that DMSP T_e values exceed ISR values in most cases. This disparity shrinks as POLITE cases occur closer to solar maximum (right side of graph).

A table containing the DMSP and Millstone Hill ISR T_e comparison values supporting Figure 25 can be found in Appendix B.

The overall average percent difference between the DMSP T_e data and all available ISR T_e estimates for 33 of the 37 cases was found to be 24.6 percent, with a standard deviation of 19.02 percent. This is roughly three times greater than the average ISR uncertainty and about six times greater than the DMSP random uncertainty (3.71 percent). This consistently large percent difference relative to ISR and DMSP uncertainties could suggest a bias in DMSP or ISR T_e measurements. DMSP and ISR T_e measurements generally become closer towards solar maximum, with percent differences decreasing from about 46 percent near solar minimum to 15 – 20 percent towards solar maximum. Table 13 below shows the breakdown of the average DMSP – ISR percent differences and standard deviations by pulse length. Scatter plots and tables presenting each case's percent difference by pulse length are found in Appendix A.

Table 13. DMSP – Millstone ISR Average Percent Differences

Pulse Length	**# of Cases**	**Avg % Diff.**	**% Diff. σ**
410 μs	31	31.30	18.95
1000 μs	16	14.12	13.39
2000 μs	22	22.77	19.39
Total Avg.		24.60	19.02

The 1000 μs cases show the smallest average percent difference of 13.39 percent. This result can be attributed to the fact that most of these cases occur closer to solar maximum, where DMSP T_e – ISR T_e agreement improved.

Photoelectron and Solar Cycle Influences on DMSP T_e Values

Referring back to Figure 25, DMSP T_e values show distinct solar zenith angle (SZA) and solar cycle related trends that are independent of spacecraft. Percent differences are smaller for conjunctions with a larger SZA, including those cases occurring during darkness, when the solar zenith angle exceeded 118 degrees. This trend is most evident during POLITE campaigns 1-5 in particular, as DMSP flyovers with a smaller SZA (corresponding to more frequent photoionization and more photoelectrons produced) resulted in much higher T_e values than both corresponding ISR T_e values and neighboring DMSP T_e values within the same POLITE campaign. Analysis of POLITE 1-5 conjunctions with DMSP T_e values (from Figure 25) that are clearly higher than the main T_e grouping revealed an average SZA of 66 degrees, with DMSP T_e values averaging 46 percent higher than average ISR T_e values (See Table 14). On the other hand, the remaining conjunctions with DMSP T_e values closer to ISR T_e values during POLITEs 1-5 averaged a 103-degree SZA and 19 percent difference (see Table 15). This trend suggests a pronounced photoelectron impact on T_e, where photoelectrons are collected by the electron probe, and lead to elevated T_e measurements. This photoelectron influence on DMSP T_e measurements decreased towards solar maximum as ambient electron densities increasd (see discussion on pg. 33). In fact, the 19 percent difference from those cases during POLITEs 1-5 not suspected for photoelectron contamination was quite consistent with the overall percent difference results (15 – 20 percent) for all cases towards solar maximum.

Table 14. Millstone Hill POLITE 1-5 Cases: "Low" Solar Zenith Angle

Case Number	Satellite	SZA(°)	DMSP T_e	ISR Avg. T_e	DMSP - ISR
M2-1	F12	66	4988.4	2958.0	2030.4
M2-2	F12	65	4522.9	2600.3	1922.6
M2-3	F12	65	4716.7	3181.5	1535.2
M3-1	F12	32	4356.7	2997.1	1359.6
M3-3	F13	71	4071.7	2530.6	1541.2
M3-4	F13	67	3856.4	2658.0	1198.4
M4-2	F12	75	4223.8	3146.3	1077.6
M4-3	F14	70	4146.2	3109.1	1037.1
M4-5	F14	75	4404.2	3065.2	1339.0
M5-2	F13	71	4084.4	3146.6	937.9
M5-3	F13	69	3821.7	2857.0	964.7
Mean		66	4290.3	2931.8	1358.5
Std. Deviation		11.8	355.5	236.7	370.7
% Difference					**46.34%**

Table 15. Millstone Hill POLITE 1-5 Cases: "High" Solar Zenith Angle

Case Number	Satellite	SZA (°)	DMSP T_e	ISR Avg. T_e	DMSP - ISR
[1]M1-1	F12	128	2921.0	2207.9	713.1
M1-2	F12	98	2809.7	3110.9	-301.2
M3-2	F12	102	3211.5	2989.9	221.6
M3-5	F12	102	3412.8	2449.2	963.6
M4-1	F13	99	2960.5	2569.5	391.0
M4-4	F13	99	2903.1	2457.7	445.4
M5-1	F14	97	2702.6	1956.0	746.6
M5-4	F14	97	2822.4	2203.9	618.5
Mean		102.8	2968.0	2493.1	474.8
Std. Deviation		10.4	233.1	394.8	390.0
% Difference					**19.05%**

Note: [1] Spacecraft in Darkness

DMSP vs. ISR T_e Comparison over Sondrestrom

Comparison of the six Sondrestrom conjunctions shows a similar trend of DMSP T_e values exceeding its corresponding extrapolated ISR 450 μs T_e value in all but one

instance. The overall DMSP T_e percent difference from ISR values was 19.15 percent with a standard deviation of 25.23 percent (see Table 16). This smaller percent

Table 16. DMSP – ISR T_e Comparison over Sondrestrom

Case #	Satellite	Solar Zenith Angle	DMSP T_e (K)	σ	450μs Ext. T_e (K)	% Diff.
[1] S2-1	F12	120°	2160.0	361.77	N/A	N/A
S3-1	F14	76°	4036.7	237.12	3134.94	28.76
S3-2	F13	63°	4320.0	332.57	3527.03	22.46
S5-1	F14	49°	3824.0	122.80	3359.83	13.82
[2] S6-1	F14	118°	1780.0	464.76	2254.97	-21.06
S8-1	F13	103°	2726.7	213.85	1740.20	56.69
S9-1	F13	103°	2100.0	504.65	1838.87	14.20
					Avg. % Diff.	**19.15**
					σ of Avg. % Diff.	**25.23**

Notes: [1] = Spacecraft in darkness

[2] Terminator Zenith Angle = 118°

difference compared to the average Millstone Hill percent difference of 24.6 percent could be misleading due to the small number of Sondrestrom cases involved and the large uncertainty involved with extrapolating Sondrestrom ISR T_e data. Both DMSP and corresponding ISR T_e measurements are higher in cases during summer in daylight with smaller solar zenith angles, than in the cases during winter with larger solar zenith angles. Figure 26 shows a graphical representation of these conjunctions. Note that the DMSP spacecraft involved in each case is shown as the last term of the case number. In Case 6-1, the one instance where the DMSP T_e is less than the extrapolated ISR T_e value, the altered mode of SSIES measurement collection at the time (POLITE 6 – see pg. 38, Item 2) could have contributed to the overly smoothed SSIES T_e values. The fact that the SSIES and ISR T_e values trace similar T_e patterns for five of the six conjunctions

suggests that both instruments are equally responsive to the surrounding ionospheric phenomena, and perhaps a similar DMSP T_e measurement bias exists at high latitudes as well. Due to only six bona-fide T_e comparisons examined over Sondrestrom, and the expected large variability of high latitude T_e over short distances, it is difficult to make any further assessments without pursuing a more comprehensive study.

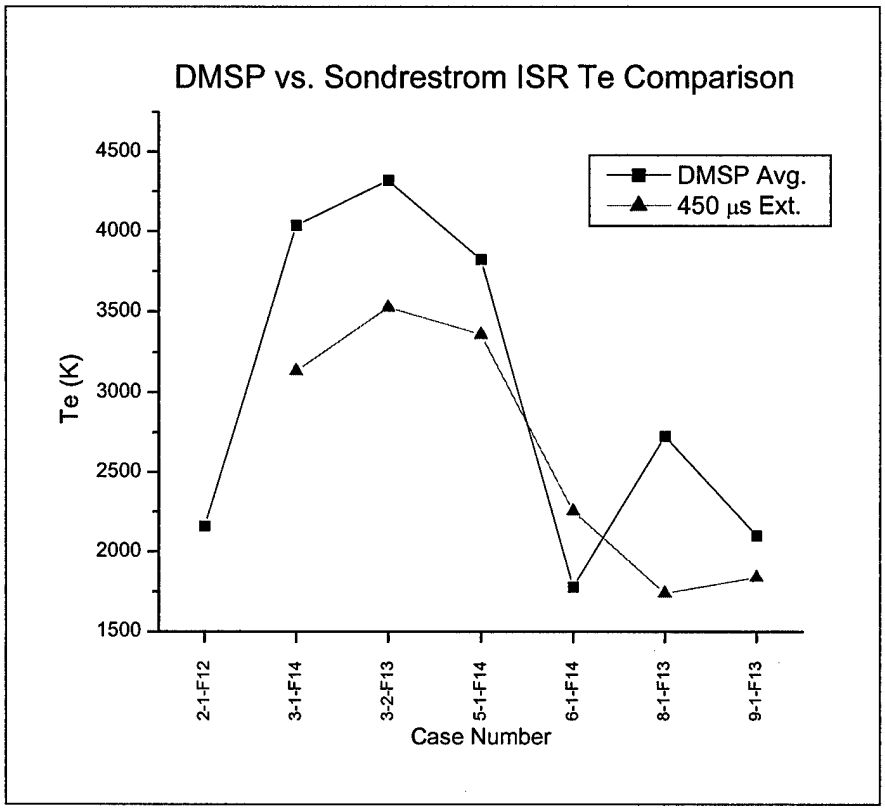

Figure 26. Conjunctions of DSMP – 450 μs ISR Extrapolated T_e Values Above Sondrestrom. DMSP values are averaged within a one-degree circle "up B" centered at 65.9 N, 311.2 E (Geographic). Note that ISR extrapolation was not possible for Case 2-1.

Unusual DMSP T_e Profiles

Closer inspection of DMSP T_e behavior along the 44 orbits containing the Millstone Hill and Sondrestrom POLITE conjunctions reveal possible instrument and

data processing related anomalies that could have distorted averaged T_e values from 14 of the conjunctions. First, Dr. Hairston cautioned that T_e values become unreliable when the SSIES SENPOT cannot remain at the plasma potential, and consequently drops to the spacecraft potential *[Hairston, private correspondence, 21 Dec 00]*. This seemed to be the case most noticeably during a considerable sector of the daylight portion of the F14 orbits during POLITE 10, and more in general from where the solar zenith angle decreases from its maximum to minimum value, from about 140 to 40 degrees. As soon as the spacecraft crossed the terminator into daylight, T_e values dropped to between 700 – 1000 K. Electron temperatures then abruptly jumped to reasonable once again when the solar zenith angle began climbing from its minimum value (~ 40 degrees). Once the zenith angle reached its maximum value (~ 140 degrees) and began decreasing, T_e values gradually decreased seemingly more in response to an unpredicted SENPOT increase than to true ionospheric variations. Figure 27 shows this pattern of T_e behavior for a F14 orbit during POLITE 10 that contains Millstone Hill case M10-1. F12 SENPOT problems seem to impact two Millstone conjunctions during earlier POLITE campaigns as well, but not as dramatically as with the F14 POLITE 10 cases (see Chapter III, Table 8).

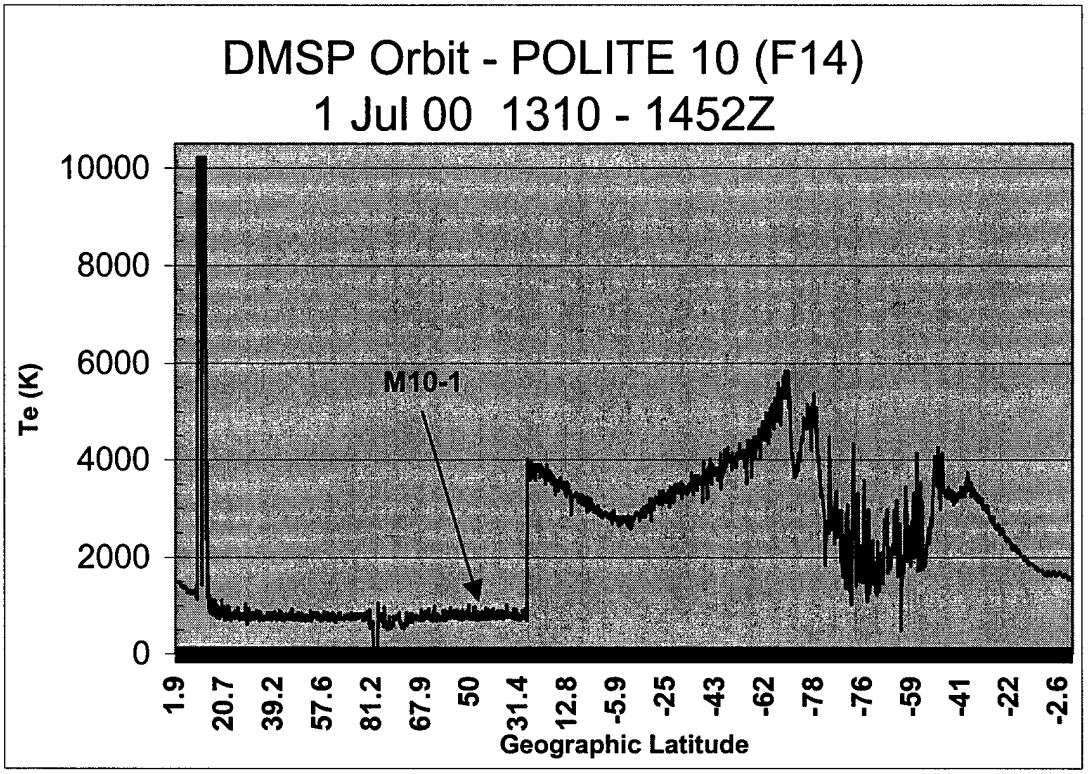

Figure 27. F14 Orbit Containing Millstone Hill Conjunction M10-1. As the spacecraft traverses the sunlit portion of its orbit (much of the Northern Hemisphere), SENPOT goes missing and T_e values drop to nominal values of 700 – 1000K. Average DMSP T_e for M10-1 is 811.0 K.

Playing more of a minor impact on results, as mentioned in Chapter III, the SSIES electron probe was in a retarded T_e measurement collection mode during the entire POLITE 6 time frame (22 – 25 November, 1998) *[Hairston, private correspondence, 21 Dec 00]*. This reduced the resolution of the T_e structure and resulted in a smoother, step-like T_e structure through the entire spacecraft orbit (see Figure 28). As another possible cause for skewed results, Dr. Sultan of AFRL advised us to be wary of F13 T_e measurements being too high during the evening pass over Millstone Hill *[Sultan, private correspondence, 26 Sep 00]*. Table 17 shows a breakdown of conjunctions possibly affected by instrument or data processing related anomalies. Note that the four cases (M8-3, M10-1, M10-4, M10-7) that show a SENPOT anomaly as a significant impact on

the resulting DMSP mean T_e were excluded from our results statistics. A significant impact is defined as an anomaly producing a DMSP T_e value more than 1500 K away from corresponding ISR T_e estimates. Evidence of anomaly impact on a case's DMSP electron temperature profile is best viewed in the DMSP T_e plots for all 37 Millstone conjunction flyovers, which are available as a separate document upon request.

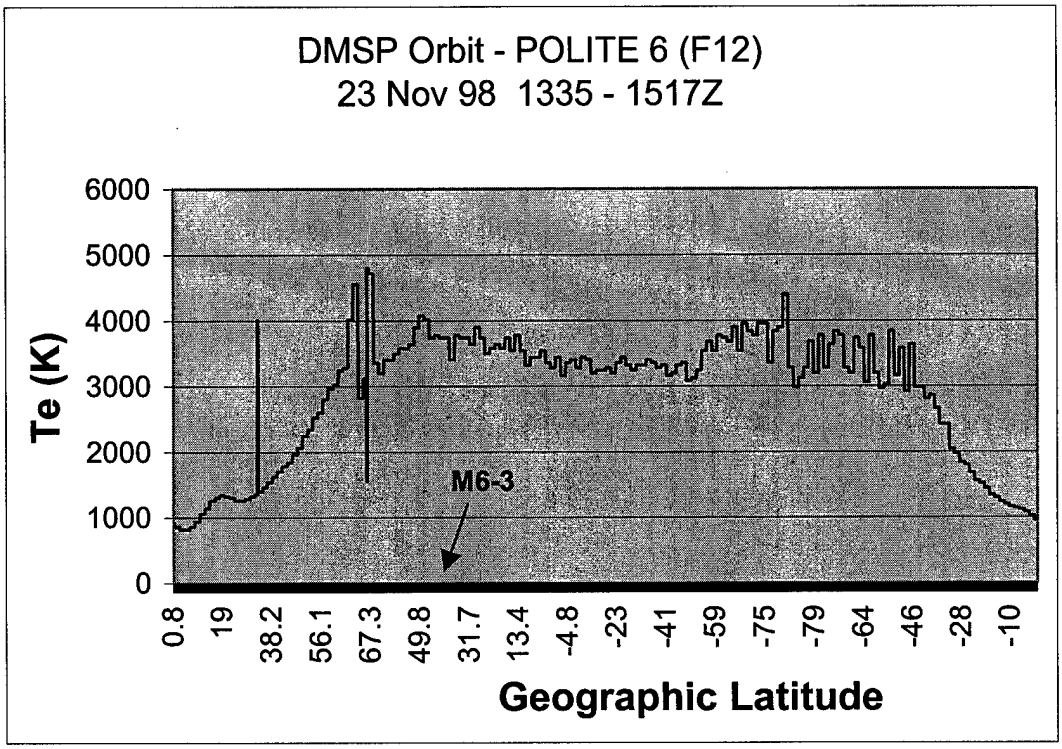

Figure 28. DMSP T_e Measurements from an Orbit During POLITE 6. A smoother, step-like profile results from a slower measurement collection mode.

Table 17. Cases with Possible Distorted T_e Results

Case	Satellite	Cause of Anomaly	Impact on T_e	Impact on ISR Comparison
M3-2	F12	SENPOT	Sporadic Fluctuations	Moderate
[1] **M8-3**	F12	SENPOT	Sporadic Fluctuations	Significant
[1] **M10-1**	F14	SENPOT	T_e 700 – 1000 K	Significant
[1] **M10-4**	F14	SENPOT	T_e 700 – 1000 K	Significant
[1] **M10-7**	F14	SENPOT	T_e 700 – 1000 K	Significant
M3-4	F13	SSIES settings	T_e too high	Moderate
M5-3	F13	SSIES settings	T_e too high	Moderate
M9-1	F13	SSIES settings	Te too high	Moderate
M10-3	F13	SSIES settings	T_e too high	Moderate
M10-6	F13	SSIES settings	T_e too high	Moderate
M6-1	F14	Slower T_e Collection Mode	Smoother Profile	Minor
M6-2	F13	Slower T_e Collection Mode	Smoother Profile	Minor
M6-3	F12	Slower T_e Collection Mode	Smoother Profile	Minor
S6-1	F14	Slower T_e Collection Mode	Smoother Profile	Minor

Note: [1] Cases Discarded for Unreliable T_e Values.

DMSP T_e Random Noise Level Results

After four of the DMSP T_e profiles were removed for probable SENPOT error, the average noise level, calculated as the standard deviation as a fraction of the mean (SDFM), of the remaining 33 data sets, turned out to be 3.71 percent. This result falls well within the quoted SSIES T_e measurement accuracy of 10 percent in Rich's *SSIES User's Guide [1994]* despite the rudimentary assumption of a linear behavior of mid latitude electron temperatures to de-trend the data. Table 18 contains a summary of SDFM results by case, where $\overline{Te_1}$ = Filtered Mean T_e and σr_1 = Standard Deviation of Filtered Residuals.

Table 18. DMSP Random Noise Level (SDFM) Calculations

Case #	Satellite	Solar Zen. Angle	Tot. Pts.	Pts. Removed	$\overline{Te_1}$ (K)	σr_1	SDFM
[4]M1-1	F12	128	41	1	2895.0	113.233	3.91%
M1-2	F13	98	29	2	2803.0	145.950	5.21%
M2-1	F12	66	31	1	5076.0	221.795	4.37%
M2-2	F12	65	41	1	4535.5	175.288	3.86%
M2-3	F12	65	36	0	4716.7	169.310	3.59%
M3-1	F12	32	18	2	4367.5	158.800	3.64%
[3]M3-2	F12	102	13	1	3345.8	286.755	8.57%
M3-3	F13	71	29	2	4097.0	122.360	2.99%
M3-4	F13	67	22	1	3833.3	121.622	3.17%
M3-5	F12	102	39	1	3425.8	189.208	5.52%
M4-1	F13	99	40	1	2952.3	124.063	4.20%
M4-2	F12	75	26	0	4223.8	172.367	4.08%
M4-3	F14	70	39	2	4175.1	150.046	3.59%
M4-4	F13	99	26	1	2912.0	87.275	3.00%
M4-5	F14	75	38	1	4421.1	153.842	3.48%
M5-1	F14	97	39	1	2709.5	107.161	3.96%
M5-2	F13	71	27	2	4092.0	57.119	1.40%
M5-3	F13	69	23	0	3821.7	180.458	4.72%
M5-4	F14	97	34	1	2830.9	106.741	3.77%
[4]M6-1	F14	130	11	1	2976.0	6.044	0.20%
M6-2	F13	97	40	3	3503.3	52.422	1.50%
M6-3	F12	70	37	0	3693.5	99.322	2.69%
[2,3,4]M7-1	F14	121	41	3	2570.5	232.428	9.04%
[4]M7-2	F12	120	27	0	2580.7	30.061	1.16%
M7-3	F13	86	24	1	3547.8	357.924	10.09%
[4]M8-1	F14	131	15	0	3129.3	66.524	2.13%
M8-2	F13	99	24	1	2987.0	97.064	3.25%
[1]M8-3	F12	75	22	0	5592.7	2045.891	36.58%
M9-1	F13	98	28	2	3333.8	77.985	2.34%
[1]M10-1	F14	40	29	1	805.7	66.780	8.29%
M10-2	F15	33	39	1	4147.9	91.625	2.21%
M10-3	F13	68	40	1	3474.9	102.686	2.96%
[1]M10-4	F14	95	22	1	771.4	53.867	6.98%
M10-5	F15	33	12	0	3895.0	113.169	2.91%
M10-6	F13	68	21	1	3315.0	90.960	2.74%
[1]M10-7	F14	95	40	1	768.7	59.210	7.70%
M10-8	F15	101	32	1	2838.7	63.944	2.25%
Avg. SDFM							**3.71%**

Notes: [1] Cases not used in SDFM average due to SENPOT error

[2] Spacecraft crosses terminator solar zenith angle (118°)

[3] Probable sporadic SENPOT error

[4] XXX = Spacecraft in dark

As the table shows, most individual noise calculations are under five percent. Six of the nine SDFM values over five percent can be at least partially attributed to SENPOT problems. No distinct trend could be detected with respect to season, however noise levels are generally about 1-2 percent smaller closer to solar max and for those cases where the spacecraft is in the dark.

Although a linear fit seemed reasonable to de-trend most data sets, as in the example in Chapter III, a few cases showed a variable T_e structure where a straight line fit was not appropriate. Also the $2\sigma r$ threshold established to remove outlying points did not always do so after just one de-trending and filtering iteration. In fact, a poor linear fit after one iteration of filtering highly variable data can still contain points which should be outliers and can also exclude points that are part of the physical trend. This can result in noise estimates that are not representative of the true data variation. Figures 29 and 30 shows the linear fits of raw and filtered T_e data for Case M7-1 that demonstrate these shortcomings. Further inspection of this case suggests that the SSIES SENPOT abruptly caused unreliable DMSPT T_e values when the spacecraft crossed into the sunlit sector of its orbit near 46 degrees N (geographic). Thus a subjective "human" analysis for such cases would help complement the aforementioned noise level determination methodology.

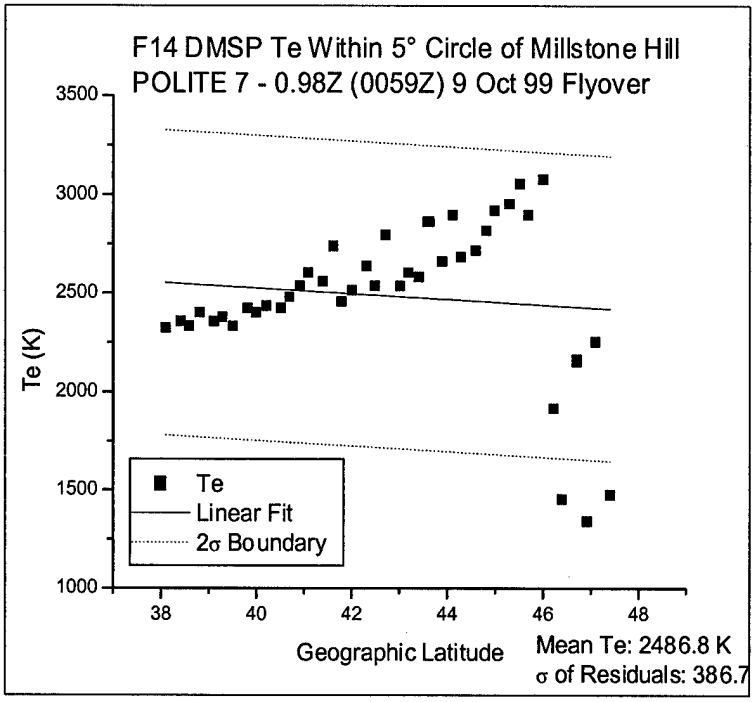

Figure 29. Initial Fit of Case M7-1 DMSP T_e Data Showing Three Outliers.

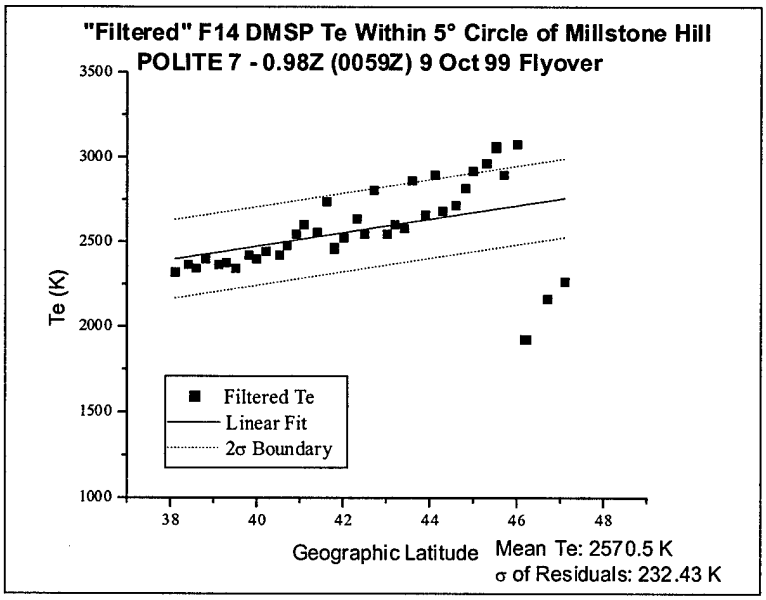

Figure 30. Poor Linear Fit of "Filtered" Data. Three of the nine points outside of the recalculated $2\sigma r$ boundary seem to be "bad" data, whereas the other six seem to follow the physical trend of the data.

In instances such as these, a simple curve fit and a second filtering iteration could have kept and removed the appropriate points. Furthermore, applying Chauvenet's Criterion to reject unreasonable measurements might have more accurately removed the appropriate outliers than our established $2\sigma r$ boundary.

Case Comparisons

Two case comparisons were performed to evaluate the consistency of DMSP Te measurements collected by different spacecraft passing over Millstone Hill within minutes of each other. Both comparisons involve F14 and F12 spacecraft and are listed in Table 19.

Table 19. Case Comparison Details

	Case	YrDay	Time (Z)	Sat.	Alt. (km)	Zen. Angle	Pts. w/in 5°	Avg. Te (K)
	M4-2	97337	1400	F14	860.56	75°	39	4146.2
Compared to:	M4-3	97337	1423	F12	847.90	70°	26	4223.8
	M7-1[1,2]	99282	0059	F14	859.22	121°	41	2486.8
Compared to:	M7-2[1]	99282	0114	F12	849.39	120°	27	2580.7

Notes: [1] = Spacecraft in dark

[2] Crosses terminator zenith angle (118°) within five-degree circle

In both instances, F12 flies over Millstone Hill about 20 minutes later at a slightly lower altitude than F14 and yields T_e values about 80 – 90 K higher than those from F14. This T_e difference is within the random noise level (3.71 percent) calculated during this research. In addition, we can probably assume steady-state ionospheric conditions during

these two periods. Therefore, the SSIES electron probes on both spacecraft seem to be taking consistent T_e measurements during these periods. Figure 31 shows how cases M7-1 and M7-2 trace similar T_e profiles approaching the terminator from darkness into sunlight. Note that T_e data was missing past 47° N (Geographic) for Case M7-2.

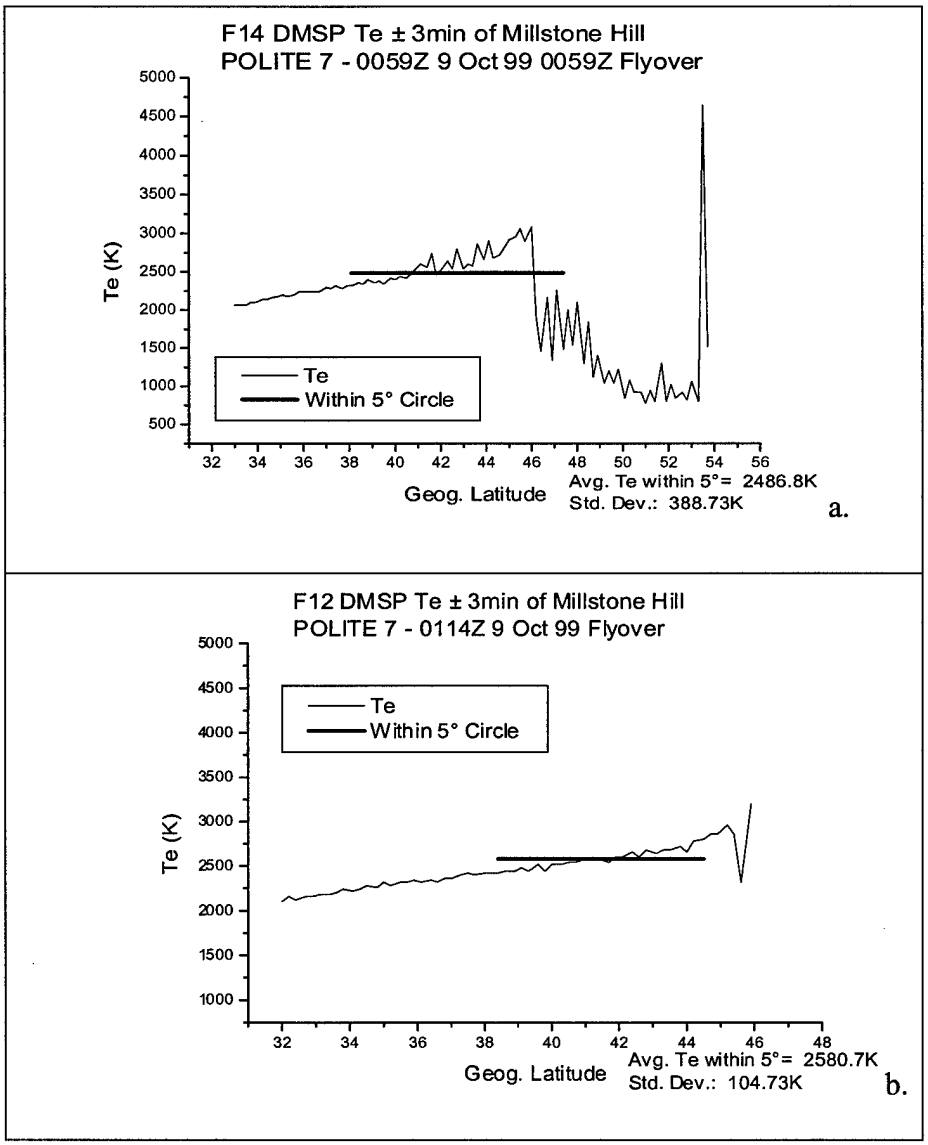

Figure 31. DMSP T_e Profile Comparison of (a) Case M7-1 against (b) Case M7-2. The mean DMSP T_e for Case M7-2 within the five-degree circle exceeds that from Case M7-1 by only 93.9 K.

Case Studies – Mid-Latitude Ionospheric Phenomena

Evidence of characteristic mid-latitude ionospheric features such as subauroral ion drifts (SAID), electron density (n_e) troughs (MT), and light ion troughs (LIT) is present in several Millstone conjunction profiles. After inspecting a 20-degree latitude range of SSIES data surrounding Millstone Hill during the 37 conjunctions, Table 20 below gives a summary of the features that occurred. Note that bad or missing RPA and SENPOT data limited the completeness of this effort.

Table 20. Case Summary of Mid Latitude Features

Case	SAID	MT	LIT	Case	SAID	MT	LIT
M1-1	X	X	X	M6-1		X	
M1-2		X	X	M6-2		X	
M2-1			X	M6-3			
M2-2			X	M7-1			
M2-3				M7-2			
M3-1				M7-3		X	
M3-2				M8-1			
M3-3				M8-2		X	
M3-4				M8-3			
M3-5				M9-1			
M4-1		X	X	M10-1			
M4-2		X	X	M10-2		X	
M4-3				M10-3		X	
M4-4		X	X	M10-4		X	
M4-5			X	M10-5		X	
M5-1				M10-6		X	
M5-2				M10-7			
M5-3				M10-8			
M5-4							

Being located equatorward of the auroral oval, Millstone Hill's location was ideal to detection of at least part of a mid-latitude n_e trough. Mid latitude troughs were mainly

identified by correlating a sloped n_e profile with a corresponding inversely related T_e profile. Figure 32 shows an example of a MT identified during a DMSP flyover during POLITE 10 (Case M10-3). Electron temperature seems to reach a general maximum where the n_e trough bottoms out.

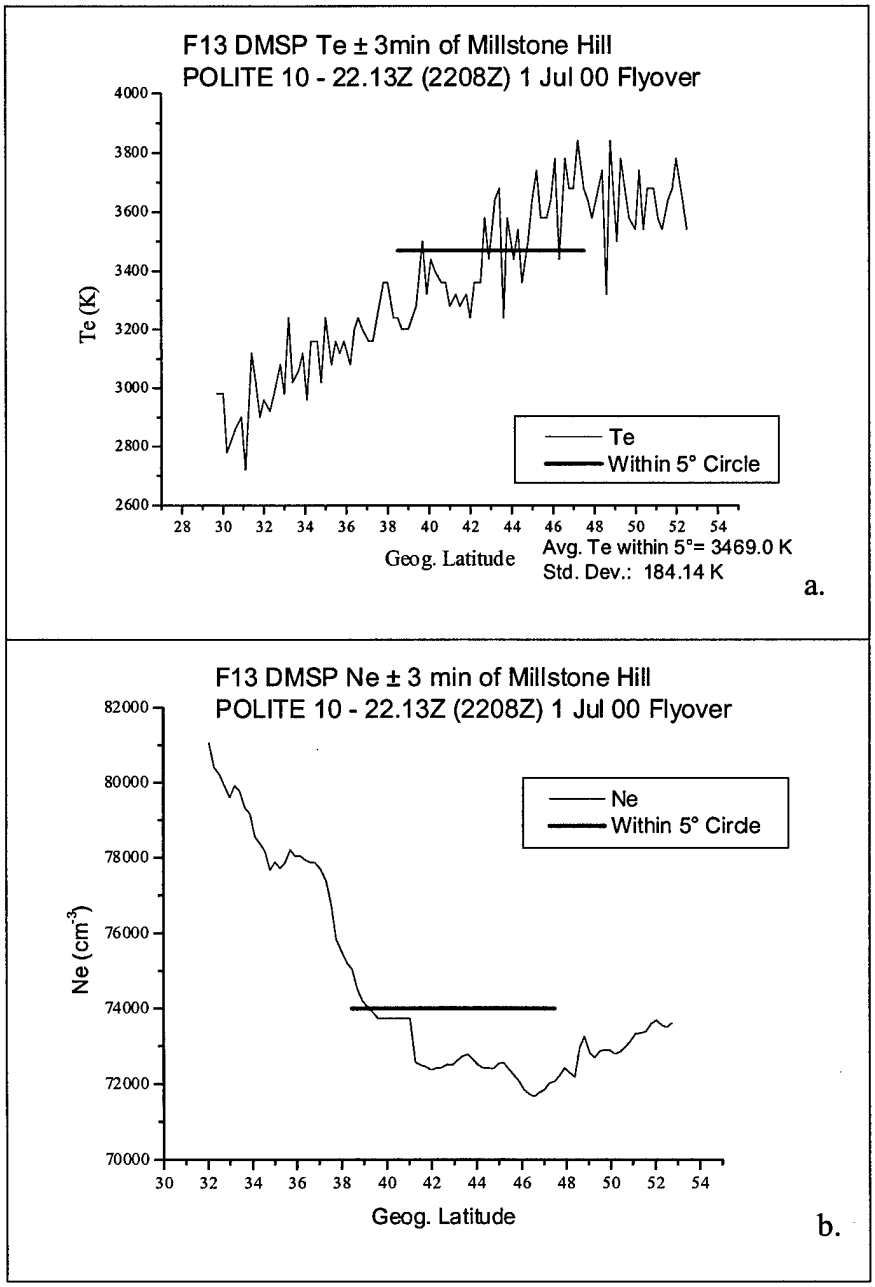

Figure 32. Case M10-3, DMSP Plots of (a) T_e and (b) n_e Showing Support for a Mid-Latitude Trough around 46°N Geographic Latitude.

The best indication of a SAID and LIT were shown in Case M1-1. Recall that a SAID is typically a region of a rapid westward ion drift which, via upward thermal conduction, can cause elevated T_e values at DMSP altitude. Meanwhile, recollect that the LIT is rapid density depletion of H^+ or He^+ that is most pronounced in the nighttime winter evening sector. All of these ingredients exist to support a SAID, LIT, and MT occurrence during Case M1-1 (See Figure 33). Note that in the ion velocity plot (b), +Vy is oriented to the left of the spacecraft's forward direction of motion, which for this case corresponds to a westward drift *[Hairston, private correspondence, 23 Aug 00]*.

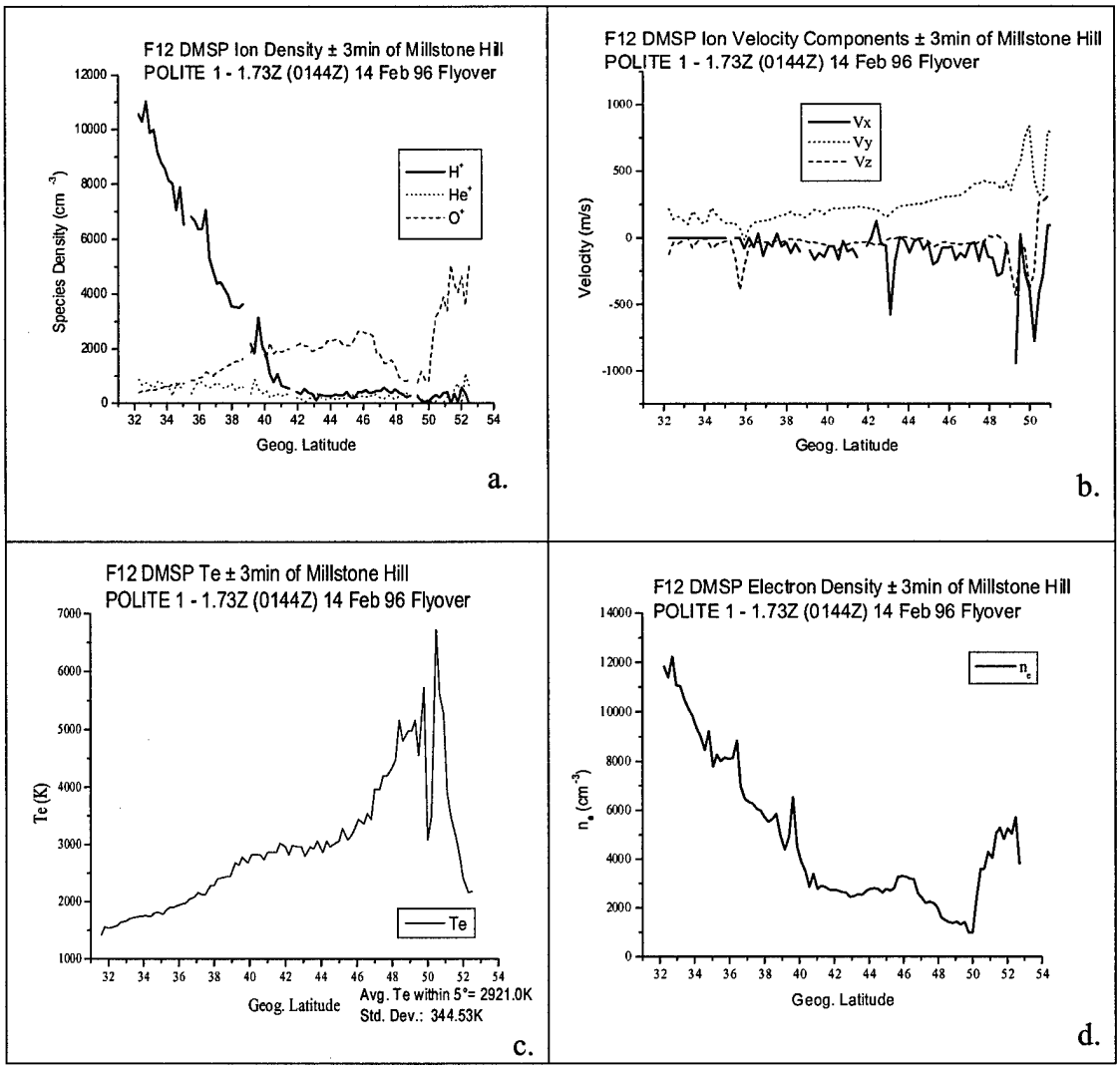

Figure 33. Simultaneous SSIES plots of (a) Ion Density, (b) Ion Velocity, (c) T_e, and (d) n_e profiles during Case M1-1 on 14 Feb 96 Showing Evidence of a LIT, SAID, and MT towards the Right Side of the Plots.

V. Summary, Conclusions and Recommendations

Summary

Geomagnetic disturbances in the near earth space environment can adversely affect numerous military and DOD systems and operations. To improve the prediction accuracy of such disturbances, the next generation of space environment forecast models (i.e. GAIM) aims to incorporate near real-time space-based and ground-based measurements into a physically realistic model field. DMSP SSIES electron temperatures represent one such space-based parameter to be ingested into GAIM. Thus the need arose to validate and assess the reliability and noise level of DMSP SSIES electron temperatures.

SSIES T_e measurements were compared against near simultaneous Millstone Hill and Sondrestrom ISR T_e measurements taken during POLITE Campaigns 1-10 spanning from Winter 1996 to Summer 2000. Incoherent Scatter Radar T_e measurements were filtered to remove highly erroneous or noisy data and then either averaged or extrapolated to DMSP altitude to determine a comparison value. Conjunction criteria similar to that used in the Sultan and Rich *[2000]* recent ion density study led to 37 Millstone Hill comparison cases, while a more restrictive criteria resulted in seven possible Sondrestrom cases. Percent differences were then calculated between each case's T_e comparison values.

A first guess linear regression was then performed on the 37 DMSP Millstone Hill flyovers to estimate random noise level as the standard deviation as a fraction of the

mean. This approach was not appropriate to approximate the highly variable T_e structure at auroral latitudes, thus a noise level was not computed for the Sondrestrom flyovers.

Conclusions

For both locations, and at all available ISR pulse lengths, DMSP T_e values consistently exceeded comparable averaged ISR values. For the 37 Millstone Hill conjunctions, DMSP T_e values averaged 24.6 percent greater than Millstone ISR values. This result is nearly three times greater than the average computed Millstone ISR uncertainty. Percent differences generally were largest when the solar zenith angle was smallest, especially during solar minimum when ambient electron densities were low, suggesting a pronounced photoelectron impact on DMSP T_e values. Satellite versus radar T_e percent differences for the Millstone Hill conjunctions decreased as the solar cycle approached solar maximum. Also, percent differences were generally smaller when the conjunction region was in darkness; perhaps due to photoelectrons collected by the SSIES electron probe (when sunlit) interfering with the T_e measurement procedure and skewing resulting T_e values.

For the six Sondrestrom conjunctions, DMSP T_e values averaged 19 percent greater than ISR measurements. Although this average percent difference is smaller than that calculated for the Millstone Hill conjunctions, the Sondrestrom percent difference tally showed a four percent larger standard deviation. The smaller average percent difference result over Sondrestrom must be viewed in light of several factors. These include the highly dynamic nature of the high latitude ionosphere, the ISR T_e filtering and extrapolation routine involved working with large errors and uncertainties, and the fact

that only seven conjunctions were considered. Consequently, a more thorough T_e comparison for Sondrestrom would likely generate more trustworthy statistics. Meanwhile, the concurrent electron density study over the two ISR sites revealed average DMSP n_e measurements that were lower than average ISR n_e values, thus verifying the expected inverse T_e vs. n_e relationship for a given amount of energy *[Keyser, Thesis Draft, 2001]*.

Average DMSP random noise over Millstone Hill for the 37 cases was computed at 3.71 percent, which is well within the published SSIES T_e measurement uncertainty of ten percent. *[Rich, 1994]*. Individual conjunction noise estimates that were larger than six percent were most likely due to a SENPOT problem disrupting the T_e profile, or when our assumption of a smooth, linear T_e variation over Millstone Hill was invalid.

Major sources of error for this study included instrument anomalies existing during parts of DMSP orbits, the random DMSP noise level, the uncertainty involved with averaging or extrapolating ISR values to DMSP altitudes, and the inherent T_e uncertainty already accompanying the ISR T_e values, especially at higher altitudes. The fact that the ISR T_e values relied upon a number of key assumptions, together with the frequent highly uncertain ISR T_e behavior at DMSP altitude, showed that such measurements were not quite as reliable a standard as anticipated. We accounted for the aforementioned sources of error as best we could by filtering out "bad" ISR T_e values and removing four Millstone conjunctions from our calculations due to clearly unreliable DMSP T_e values. Thus, we remain confident in our findings. Given that SSIES measured T_e consistently exceed near-simultaneous ISR measured T_e, and that different spacecraft with similar flyover times and solar zenith angles over Millstone Hill show

comparable T_e values (within the computed random DMSP noise level), there is a possibility that some sort of DMSP T_e or ISR T_e bias exists.

Recommendations

This research has only scratched the surface of accurately validating SSIES measured parameters to be ingested into GAIM. The first step from here is to coordinate our existing results with experts at UTD, AFRL, and Millstone Hill to discover the source of the apparent T_e bias between ISR and the DMSP SSIES. This will surely involve further ISR vs. SSIES data comparisons encompassing other latitude ranges and a wider range of geomagnetic activity. Incoherent Scatter Radar data from Arecibo, Puerto Rico and Jicamarca, Peru would make low latitude comparisons possible, while European Incoherent Scatter (EISCAT) data from northern Scandinavian stations, and a more thorough Sondrestrom SSIES – ISR comparison, would expand the comparison to high latitudes. Since most cases in this study occurred during geomagnetic quiet conditions ($Kp < 3$), examining cases during periods of more active geomagnetic storm levels will broaden the comparison database as well. With a more comprehensive database of DMSP vs. ISR measurement comparison results with respect to latitude, solar cycle, solar illumination, and storm level, any bias that might exist should emerge.

Since ISR returns become quite weak at higher altitudes, especially those returns above 700 km and with SN ratios less than 0.1, estimating an ISR T_e value at DMSP altitude involved a large uncertainty. Consequently, more *in-situ* measurements by rockets or other spacecraft need to be performed to reduce measurement uncertainty at DMSP altitude.

Our DMSP T_e noise level study was limited to a linear fit, mid-latitude estimate. Ideally, random noise error needs to be approximated with respect to latitude, solar illumination, solar cycle and geomagnetic activity. A start toward this goal would be to de-trend and compute noise levels from T_e data from other latitude sectors of the 1147 DMSP orbits available for this study. As a start in that direction, upon sampling T_e data from various sections of DMSP orbits, the equation: $y = a + bx^3$ best fit the data in nearly one third of 32 cases. GAIM best models physical parameters exhibiting slowly varying ionospheric behavior as at low and mid-latitudes. At high latitudes, the Kalman filter would treat highly varying ionospheric parameters over short distances as noise *[Sojka, private correspondence, 15 Nov 00]*. Thus a more spatially sensitive routine must be considered to account for the short scale lengths of high latitude ionospheric phenomena.

With the trend of next generation space environment models relying upon assimilating spaced based measurements, it is imperative to encourage future SSIES parameter validations and to continue to promote near-real time telemetry of such parameters. A better understanding of SSIES characteristics will greatly benefit AFRL modeling efforts as well as future research involving DMSP space environment data. Since GAIM has the capacity to ingest new data types as they become available, expanding the stock of ionospheric measurements can only benefit the GAIM initiative. As a result, future space environment forecasts models such as GAIM will become more accurate at predicting impending geomagnetic disturbances that could impact military and DoD systems and operations.

Appendix A: DMSP vs. Millstone Hill ISR Percent Difference Results

Table 21. DMSP vs. Millstone Hill ISR Percent Difference Results

Case #	Sat.	DMSP Mean T_e (K)	410 μs T_e (K)	% Diff.	1000 μs T_e (K)	% Diff.	2000 μs T_e (K)	% Diff.
M1-1	F12	2921.0	2207.91	32.30	No Data		3602.15	-18.91
M1-2	F13	2809.7	*		No Data		3110.90	-9.68
M2-1	F12	4988.4	2957.98	68.64	*		*	
M2-2	F12	4522.9	2600.31	73.94	*		*	
M2-3	F12	4716.7	2890.01	63.21	*		3473.57	35.79
M3-1	F12	4356.7	3088.92	41.04	*		2905.23	49.96
M3-2	F12	3345.8	2905.32	15.16	3074.40	8.83	*	
M3-3	F13	4071.7	2530.55	60.90	*		*	
M3-4	F13	3856.4	*		*		2658.01	45.09
M3-5	F12	3412.8	2225.94	53.32	2672.40	27.71	*	
M4-1	F13	2960.5	2037.91	45.27	3101.05	-4.53	*	
M4-2	F12	4146.2	3252.33	27.48	*		3040.17	36.38
M4-3	F14	4223.8	2919.14	44.69	*		3298.97	28.03
M4-4	F13	2903.1	2457.66	18.12	*		*	
M4-5	F14	4404.2	3065.20	43.68	*		*	
M5-1	F14	2702.6	1985.81	36.10	2139.20	26.34	1748.98	54.52
M5-2	F13	4084.4	3095.07	31.96	*		3198.03	27.72
M5-3	F13	3821.7	2773.87	37.78	3028.57	26.19	2768.52	38.04
M5-4	F14	2822.4	2219.99	27.14	2266.20	24.54	2125.41	32.79
M6-1	F14	2974.5	2888.39	2.98	*		*	
M6-2	F13	3455.0	2551.80	35.39	*		*	
M6-3	F12	3693.5	3158.72	16.93	3131.14	17.96	3156.74	17.00
M7-1	F14	2486.8	2428.68	2.39	2475.00	0.48	2364.49	5.17
M7-2	F12	2580.7	2349.75	9.83	2456.94	5.04	2357.10	9.49
M7-3	F13	3505.8	3264.78	7.38	*		3269.50	7.23
M8-1	F14	3129.3	2548.46	22.79	3802.60	-17.71	3380.70	-7.44
M8-2	F13	3005.8	2742.37	9.61	*		*	
[1] **M8-3**	F12	**5592.7**	3205.74		3014.86		3184.45	
M9-1	F13	3318.6	2511.42	32.14	2766.80	19.94	2657.60	24.87
[1] **M10-1**	F14	**811.0**	3283.46		3576.95		3291.50	
M10-2	F15	4144.6	3446.84	20.24	3637.09	13.95	3412.61	21.45
M10-3	F13	3469.0	3010.32	15.24	3209.01	8.10	3066.39	13.13
[1] **M10-4**	F14	**779.1**	2305.00		2376.51		2218.76	
M10-5	F15	3895.0	3105.89	25.41	3166.29	23.01	3066.52	27.02
M10-6	F13	3305.7	2801.96	17.98	2868.91	15.22	2704.28	22.24
[1] **M10-7**	F14	**772.0**	2325.14		2437.31		2312.87	
M10-8	F15	2839.4	2161.87	31.34	2170.73	30.80	2013.95	40.99
Cases				32		17		23
Avg. % Diff.				32.65		18.32		25.07
Avg. % Diff. σ				20.15		21.63		21.92

Notes: * T_e Comparison Value Not Available

[1] Percent Difference Not Calculated Due to Suspected SENPOT Error

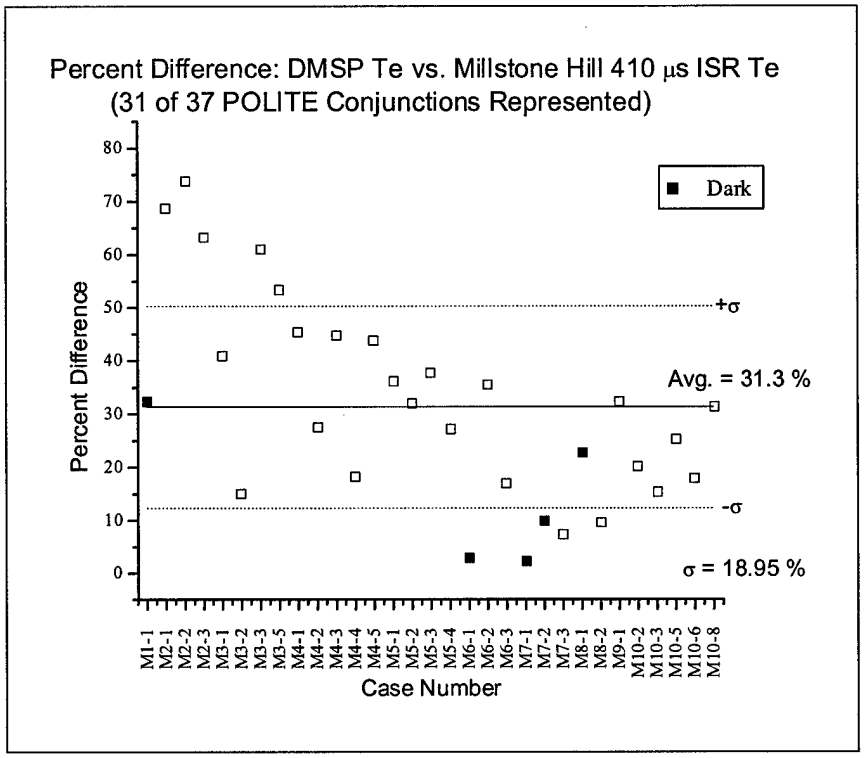

Figure 34. DMSP vs. Millstone Hill 410 μs ISR T_e Percent Difference Case Summary

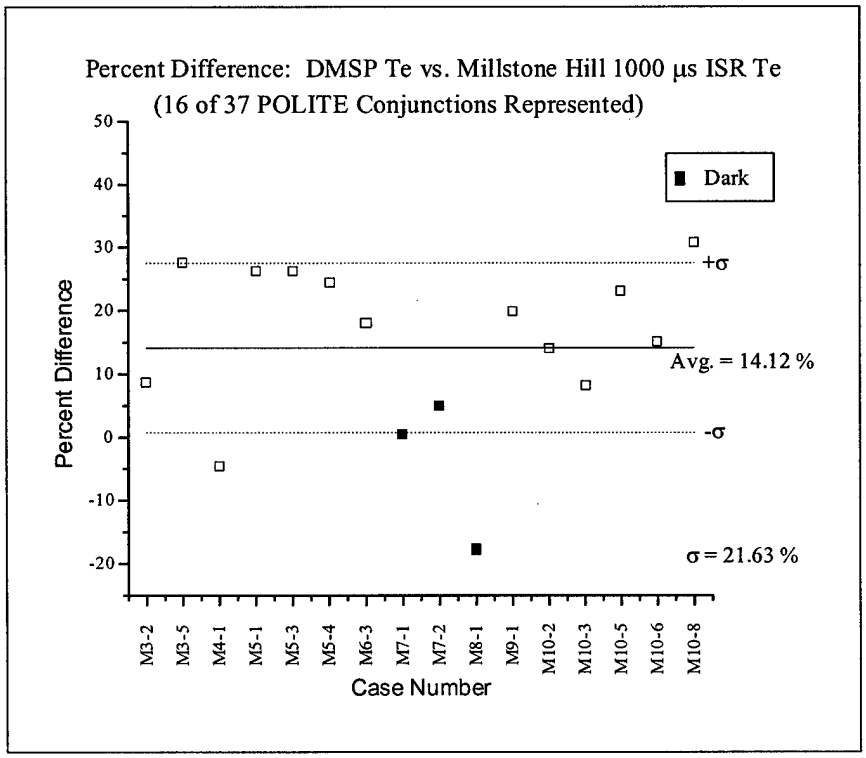

Figure 35. DMSP vs. Millstone Hill 1000 μs ISR T_e Percent Difference Case Summary

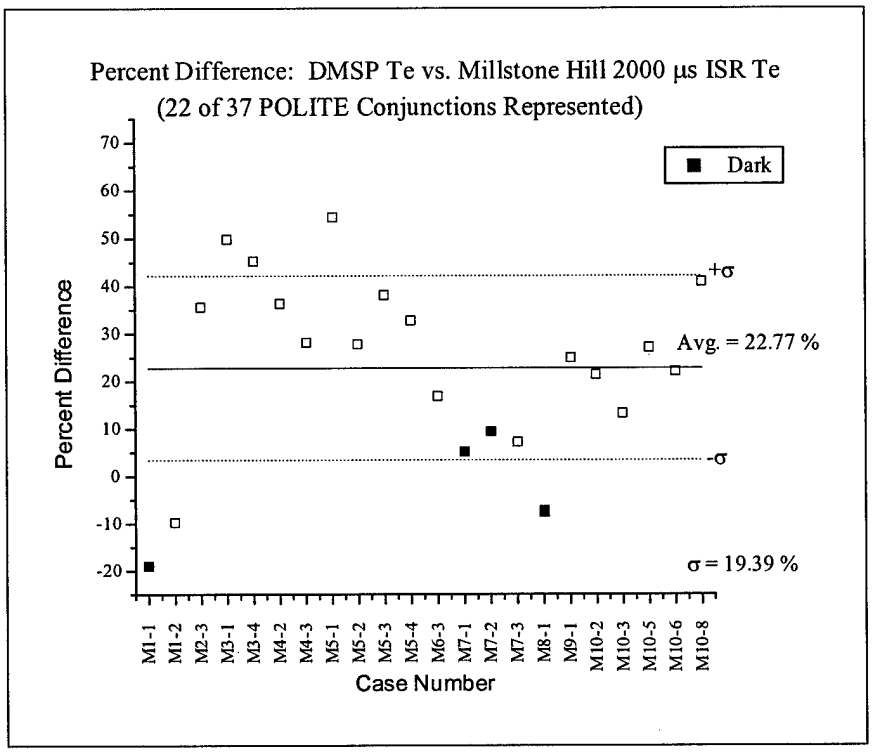

Figure 36. DMSP vs. Millstone Hill 2000 μs ISR T_e Percent Difference Case Summary

Appendix B: DMSP vs. Millstone Hill ISR T_e Comparison Values

Table 22. DMSP vs. Millstone ISR T_e Comparison Values

Case #	Space-craft	Zenith Angle	Avg Kp	DMSP Avg. T_e (K)	410μs Ext. T_e	1000 μs Avg. Te	Avg. Error	2000 μs Avg. T_e	Avg. Error
M1-1	F12	128	4.3	2921.0	2207.91	No Data		[2] 3602.15	154.15
M1-2	F13	98	3.3	2809.7	*	No Data		[1] 3110.90	222.40
M2-1	F12	66	1.0	4988.4	2957.98	*		*	
M2-2	F12	65	2.0	4522.9	2600.31	*		*	
M2-3	F12	65	1.8	4716.7	2890.01	*		3473.57	450.17
M3-1	F12	32	1.7	4356.7	3088.92	*		2905.23	308.40
M3-2	F12	102	2.0	3211.5	2905.32	[1] 3074.40	239.75	*	
M3-3	F13	71	1.0	4071.7	2530.55	*		*	
M3-4	F13	67	1.0	3856.4	*	*		2658.01	279.74
M3-5	F12	102	1.0	3412.8	2225.94	[1] 2672.40	243.05	*	
M4-1	F13	99	1.3	2960.5	2037.91	[1,2] 3101.05	277.05	*	
M4-2	F14	75	2.0	4146.2	3252.33	*		3040.17	424.67
M4-3	F12	70	2.0	4223.8	2919.14	*		3298.97	454.17
M4-4	F13	99	1.3	2903.1	2457.66	*		*	
M4-5	F14	75	1.3	4404.2	3065.20	*		*	
M5-1	F14	97	2.0	2702.6	1985.81	2139.20	237.86	1748.98	137.29
M5-2	F13	71	1.7	4084.4	3095.07	*		3198.03	357.07
M5-3	F13	69	2.0	3821.7	2773.87	3028.57	314.05	2768.52	139.91
M5-4	F14	97	0.7	2822.4	2219.99	2266.20	269.96	2125.41	127.56
M6-1	F14	130	2.7	2974.5	2888.39	*		*	
M6-2	F13	97	2.0	3455.0	2551.80	*		*	
M6-3	F12	70	3.0	3693.5	3158.72	3131.14	327.80	3156.74	248.85
M7-1	F14	121	0.7	2486.8	2428.68	2475.00	308.03	2364.49	153.89
M7-2	F12	120	0.7	2580.7	2349.75	2456.94	300.83	2357.10	160.23
M7-3	F13	86	1.0	3505.8	3264.78	*		3269.50	334.13
M8-1	F14	131	2.0	3129.3	2548.46	[1] 3802.60	431.60	3380.70	409.87
M8-2	F13	99	1.3	3005.8	2742.37	*		*	
M8-3	F12	75	2.0	5592.7	3205.74	3014.86	353.60	3184.45	256.8
M9-1	F13	98	3.3	3318.6	2511.42	2766.80	242.7	2657.60	111.2
M10-1	F14	40	1.0	811.0	3283.46	3576.95	373.36	3291.50	198.08
M10-2	F15	33	1.0	4144.6	3446.84	3637.09	419.75	3412.61	189.27
M10-3	F13	68	2.3	3469.0	3010.32	3209.01	186.32	3066.39	97.81
M10-4	F14	95	1.1	779.1	2305.00	2376.51	156.68	2218.76	70.71
M10-5	F15	33	1.0	3895.0	3105.89	3166.29	307.09	3066.52	138.30
M10-6	F13	68	1.0	3305.7	2801.96	2868.91	164.75	2704.28	89.00
M10-7	F14	95	2.0	772.0	2325.14	2437.31	140.64	2312.87	74.31
M10-8	F15	101	2.0	2839.4	2161.87	2170.73	143.50	2013.95	66.07
Cases				37	35	20		26	

Notes: * N/A

[1] Based upon only two profiles

[2] SN ratio << 0.1

xxx : Conjunction in Dark (Terminator Zenith Angle = 118°)

Bibliography

Anderson, P. C., R. A. Heelis, and W. B. Hanson. "The Ionospheric Signatures of Rapid Subauroral Ion Drifts," Journal of Geophysical Research, Vol 96, No. A4: 5785 – 5792 (April 1991).

Emery, B. A. and R. M. Barnes. The NCAR CEDAR Database Catalogue. Boulder, CO: National Center For Atmospheric Research, June 2000.

Erickson, P. J., "The Millstone Hill Observatory," n. pag. http://www.haystack.mit.edu/mhrobs/instrument_summary.html#MHISR. 21 June 1995.

Erickson, P. J. "POLITE Campaign Home Page," n. pag. http://www.haystack.edu/polite/polite_campaigns.html. 16 June 1997.

Erickson, P. J. "Millstone Hill Data from POLITE Campaigns 9 and 10 to follow." Electronic Message. 1459Z, 14 September 2000.

Erickson, P. J. "Re: AFIT Study." Electronic Message. 2128Z, 22 September 2000.

Erickson, P. J. "Re: Thoughts on Millstone Hill Data from AFIT." Electronic Message. 1903Z, 13 October 2000.

Evans, J. V. "High-Power Radar Studies of the Ionosphere," Proceeding of the IEEE, Vol. 63, No. 12: 1636-1650 (December, 1975).

Foster, John C. "Incoherent Scatter Radar Tutorial." Incoherent Scatter Radar Background Information via Millstone Hill Homepage. n. pag. http://www.haystack.mit.edu/midas/inscal.html. 16 January 2001.

Gorczyca, A. "Millstone Hill Observatory," Homepage. n. pag. http://www.haystack.mit.edu/homepage.html. 13 September 1999.

Hairston, M., "Explanation of DMSP data (R-files)." Electronic Message. 1739Z, 23 August 2000.

Hairston, M., "Re: 22 – 25 Nov 1998 (POLITE 6) DMSP data problem." Electronic Message. 2218Z, 21 December 2000.

Hargreaves, J. K. The Solar-Terrestrial Environment, London: Cambridge University Press, 1992.

"Incoherent Scatter." Incoherent Scatter Radar Background Information on EISCAT Web Site. n. pag. http://www.eiscat.uit.no/is-methods.html. 15 December 2000.

Keyser, Herbert L. Validation and Characterization of Ionospheric Densities Measured by DMSP. MS Thesis (Draft), AFIT/ENP/GAP/01M-05. School of Engineering and Management, Air Force Institute of Technology (AU), Wright-Patterson AFB, OH, January 2001.

McCready, M., "POLITE 8 & 9 Sondrestrom data." Electronic Message. 2107Z, 25 October 2000.

Mathiesen, B. "Error Analysis Tutorials." Link via U. of Michigan Physics Labs. n. pag. http://www.physics.lsa.umich.edu/IP-LABS. 11 October 2000.

Miller, N. J. "The Main Electron Trough During the Rising Solar Cycle," Journal of Geophysical Research, Space Physics, Vol. 75, No. 34: 7175-7181, (December, 1970)

Moffett, R. J. and S. Quegan. "The mid-latitude trough in the electron concentration of Ionospheric F-layer: a review of observations and modelling," Journal of Atmospheric and Terrestrial Physics, Vol. 45, No. 5: 315 – 343 (November 1982).

Press, W. H., S. A. Teukolsky, W. T. Vetterling, and B. P. Flanery. Numerical Recipes in Fortran 90: The Art of Parallel Scientific Computing, New York: 1996.

Rees, M. H. Physics and Chemistry of the Upper Atmosphere, London: Cambridge University Press, 1989.

Rich, F. Users Guide for the Topside Ionospheric Plasma Monitor (SSIES, SSIES-2, and SSIES-3) on Spacecraft of the Defense Meteorological Satellite Program (DMSP). Volume 1: Technical Description, PL-TR-94-2187: (June 1994).

Rich, F. "DMSP: General Information, Data Availability and SSIES - Thermal Plasma & Electric Field," n. pag. http://www-sbp.plh.af.mil/projects/dmsp/dmspssies.html. 4 October 2000.

Rishbeth, H. "Basic Physics of the Ionosphere: A Tutorial Review," Journal of the Institution of Electronic and Radio Engineers, Vol. 58, No. 6 (Supplement), S207 - S223. (September – December 1988).

Schunk, R. W., P. M. Banks, and W. J. Raitt, "Effects of Electric Fields and Other Processes Upon the Nighttime High-Latitude *F* Layer," Journal of Geophysical Research, Vol. 81, No. 19: 3271 – 3282 (July 1976).

Schunk, R. W., and A. F. Nagy. Ionospheres: Physics, Plasma Physics, and Chemistry. New York: Cambridge University Press, 2000.

Schunk, R. W., and J. J. Sojka. "Global Assimilation of Ionospheric Measurements Proposal," Utah State University, 1999.

Sojka, J. J. "Thesis Comments." Electronic Message. 1721Z, 8 February 2001.

Sojka, J. J. "GAIM – DMSP Errors." Handout. 15 November 2000.

Sultan, P. J., and F. J. Rich. "Validation of DMSP SSIES Ion Density Measurements with Ground-Based Incoherent Scatter Radar," Draft Document (2000).

Sultan, P.J. "DMSP Temperature Data." Electronic Message. 1522Z, 26 September 2000.

Tascione, T. F. An Introduction to the Space Environment, Second Edition. Malabar, FL: Krieger Publishing Co., 1994.

Taylor, H. A. Jr., "The Light Ion Trough," Planetary Space Science, 20: 1593 – 1605 (21 February 1972).

Taylor, H. A. Jr., "The Light Ion Trough, the Main Trough, and the Plasmapause," Journal of Geophysical Research, 77: 6716 – 1623 (December 1972).

Thayer, J., "Sondrestrom IS Radar," n. pag. http://cedarweb.hao.ucar.edu/instr/son.html. 28 December 2000.

URSI Incoherent Scatter Radar Working Group, "Incoherent Scatter Radars," Map of ISR Sites, n. pag. http://www.haystack.edu/iswg/iswg.html. 12 January 2001.

Vita

Captain Bradford S. Green was born in Washington, D.C. and raised in Bethesda, Maryland. He graduated from Walt Whitman High School in June 1988. Capt Green attended the College of William of Mary for two years (1988-1990) and then transferred to the University of Virginia, where he graduated with a Bachelor of Arts degree in Environmental Science in May 1992. He was commissioned as a weather officer through AFROTC Detachment 145 at Florida State University on 1 May 1993.

In October 1993, Captain Green was assigned as a Weather Support Team Chief at the European Forecast Unit, Traben-Trarbach, Germany. There he supervised production of routine and contingency forecast and warning products for the European Theater. In August 1995, Capt Green was reassigned as a Wing Weather Officer to the 48th Fighter Wing, RAF Lakenheath, United Kingdom, where he provided tailored weather support to three F-15 squadrons and the base community. In July 1997, Capt Green was reassigned as a Meteorological and Oceanographic (METOC) Staff Officer at United States European Command (USEUCOM), Stuttgart, Germany. There he coordinated, provided and directed meteorological and oceanographic (METOC) support for numerous theater contingencies, including Operation ALLIED FORCE in 1999.

Capt Green arrived at the Air Force Institute of Technology in August 1999 to pursue a Masters Degree in Space and Solar Sciences. Upon graduation, he will be assigned to the Air Force Weather Agency, Offutt AFB, Nebraska.

REPORT DOCUMENTATION PAGE

Form Approved
OMB No. 074-0188

1. REPORT DATE *(DD-MM-YYYY)*	2. REPORT TYPE	3. DATES COVERED *(From – To)*
09-03-2001	Master's Thesis	Jun 2000 – Mar 2001

4. TITLE AND SUBTITLE

VALIDATION AND ASSESSMENT OF DMSP ELECTRON TEMPERATURES IN THE TOPSIDE IONOSPHERE

5a. CONTRACT NUMBER

5b. GRANT NUMBER

5c. PROGRAM ELEMENT NUMBER

6. AUTHOR(S)

Green, Bradford S., Captain, USAF

5d. PROJECT NUMBER

5e. TASK NUMBER

5f. WORK UNIT NUMBER

7. PERFORMING ORGANIZATION NAMES(S) AND ADDRESS(S)

Air Force Institute of Technology
Graduate School of Engineering and Management (AFIT/ENP)
2950 P Street, Building 640
WPAFB OH 45433-7765

8. PERFORMING ORGANIZATION REPORT NUMBER

AFIT/GAP/ENP/01M-03

9. SPONSORING/MONITORING AGENCY NAME(S) AND ADDRESS(ES)

HQAFWA/XOGS
106 Peacekeeper Dr. Suite 2N3
Offutt AFB, OH 68113 DSN: 272-4102

10. SPONSOR/MONITOR'S ACRONYM(S)

11. SPONSOR/MONITOR'S REPORT NUMBER(S)

12. DISTRIBUTION/AVAILABILITY STATEMENT

APPROVED FOR PUBLIC RELEASE; DISTRIBUTION UNLIMITED.

13. SUPPLEMENTARY NOTES

14. ABSTRACT

Geomagnetic disturbances in the near earth space environment can adversely affect numerous military and Department of Defense (DoD) systems and operations. To improve the prediction accuracy of such disturbances, the next generation of space environment forecast models aims to automatically ingest real-time ionospheric measurements. This research validates and assesses one such measurement – the Defense Military Satellite Program (DMSP) measured electron temperature (T_e).

DMSP T_e data were validated against near simultaneous incoherent scatter radar (ISR) T_e measurements from Millstone Hill, MA and Sondrestrom, Greenland between Winter 1996 and Summer 2000. Of the 37 Millstone and six Sondrestrom conjunctions compared, DMSP T_e values exceeded ISR T_e values by an average of about 25 percent, which is nearly three times the mean ISR uncertainty. DMSP vs. ISR T_e percent differences were smallest during solar maximum, increasing towards solar minimum, likely due to photoelectron influence on DMSP T_e measurements. In some cases, instrument related anomalies produced unreliable measurements. Based on an assumed linear T_e behavior at mid latitudes, the average DMSP T_e random noise level above Millstone Hill was estimated at about four percent, falling well within the published T_e measurement accuracy. A more comprehensive comparison extending to other sectors of the DMSP orbit is required to further validate the root cause of the DMSP T_e - ISR T_e offset.

15. SUBJECT TERMS

Electron Temperature (T_e), DMSP, Incoherent Scatter Radar (ISR), SSIES, POLITE, Millstone Hill, Sondrestrom, Electron Probe, Solar Zenith Angle, Conjunction, Percent Difference

16. SECURITY CLASSIFICATION OF:			17. LIMITATION OF ABSTRACT	18. NUMBER OF PAGES	19a. NAME OF RESPONSIBLE PERSON
a. REPORT	b. ABSTRACT	c. THIS PAGE			Maj Devin J. Della-Rose, ENP
U	U	U	UU	113	19b. TELEPHONE NUMBER *(Include area code)* (937) 255-3636, Ext. 4514

Standard Form 298 (Rev. 8-98)
Prescribed by ANSI Std. Z39-18

Form Approved
OMB No. 074-0188